Arteriovenous fistula-induced cardiac remodeling shows cardioprotective features in mice

Shin-Rong Lee, MD, PhD,[a,b,c] Stephanie Thorn, PhD,[c] Nicole Guerrera, RDCS,[c] Luis Gonzalez, BS,[b] Ryosuke Taniguchi, MD, PhD,[b] John Langford, MD,[a,b] Albert J. Sinusas, MD,[b,c,d] *and* Alan Dardik, MD, PhD,[a,b,e]
New Haven and West Haven, Conn

ABSTRACT

Objective: Arteriovenous fistulae (AVF) placed for hemodialysis have high flow rates that can stimulate left ventricular (LV) hypertrophy. LV hypertrophy generally portends poor cardiac outcomes, yet clinical studies point to superior cardiac-specific outcomes for patients with AVF when compared with other dialysis modalities. We hypothesize that AVF induce physiologic cardiac hypertrophy with cardioprotective features.

Methods: We treated 9- to 11-week-old C57Bl/6 male and female mice with sham laparotomy or an aortocaval fistula via a 25G needle. Cardiac chamber size and function were assessed with serial echocardiography, and cardiac computed tomography angiography. Hearts were harvested at 5 weeks postoperatively, and the collagen content was assessed with Masson's trichrome. Bulk messenger RNA sequencing was performed from LV of sham and AVF mice at 10 days. Differentially expressed genes were analyzed using Ingenuity Pathway Analysis (Qiagen) to identify affected pathways and predict downstream biological effects.

Results: Mice with AVF had similar body weight and wet lung mass, but increased cardiac mass compared with sham-operated mice. AVF increased cardiac output while preserving LV systolic and diastolic function, as well as indices of right heart function; all four cardiac chambers were enlarged, with a slight decrement in the relative LV wall thickness. Histology showed preserved collagen density within each of the four chambers without areas of fibrosis. RNA sequencing captured 19 384 genes, of which 857 were significantly differentially expressed, including transcripts from extracellular matrix-related genes, ion channels, metabolism, and cardiac fetal genes. The top upstream regulatory molecules predicted include activation of angiogenic (Vegf, Akt1), procardiomyocyte survival (Hgf, Foxm1, Erbb2, Lin9, Areg), and inflammation-related (CSF2, Tgfb1, TNF, Ifng, Ccr2, IL6) genes, as well as the inactivation of cardiomyocyte antiproliferative factors (Cdkn1a, FoxO3, α-catenin). The predicted downstream effects include a decrease in heart damage, and increased arrhythmia, angiogenesis, and cardiogenesis. There were no significant sex-dependent differences in the AVF-stimulated cardiac adaptation.

Conclusions: AVF stimulate adaptive cardiac hypertrophy in wild-type mice without heart failure or pathologic fibrosis. Transcriptional correlates suggest AVF-induced cardiac remodeling has some cardioprotective, although also arrhythmogenic features. (JVS—Vascular Science 2021;2:110-28.)

Clinical Relevance: Arteriovenous fistulae (AVF) are commonly used as access for hemodialysis in patients with end-stage renal disease. AVF induce a high-output state that is associated with long-term structural cardiac remodeling, including left ventricle hypertrophy, but this element has uncertain clinical significance. Although left ventricle hypertrophy has traditionally been associated with an increased risk of cardiovascular disease, clinical studies have suggested that cardiac-specific outcomes of patients with end-stage renal disease were better with AVF compared with other dialysis modalities. This study uses a mouse model of AVF to study the structural, functional, and molecular correlates of AVF-induced cardiac remodeling. It finds that AVF causes an adaptive cardiac hypertrophy without functional decline or fibrosis. Transcriptional correlates suggest an electrical remodeling and the upregulation of proangiogenic, procardiogenic, and prosurvival factors, implying that AVF-induced cardiac hypertrophy is potentially cardioprotective, but also arrhythmogenic.

Keywords: Arteriovenous fistulae; Cardiac remodeling; Cardiac hypertrophy; Cardioprotection

From the Department of Surgery,[a] Vascular Biology and Therapeutics Program,[b] Yale Translational Research Imaging Center,[c] and Department of Radiology and Biomedical Imaging,[d] Yale University School of Medicine, New Haven; and the Department of Vascular Surgery, VA Connecticut Healthcare Systems, West Haven.[e]

Supported the National Institutes of Health Grants R01-HL-128406 and R01-HL-144476, T32-HL-098069, and the resources and use of facilities at the Veterans Affairs Connecticut Healthcare System (West Haven, CT) and the Yale Translational Research Imaging Center (New Haven, CT) funded by NIH grants S10 OD021845 and S10 RR023602.

Author conflict of interest: none.

Presented at the American Heart Association's Scientific Sessions, Philadelphia, Pennsylvania, November 16-18, 2019.

Correspondence: Alan Dardik, MD, PhD, Yale University School of Medicine, 10 Amistad St, Room 437, PO Box 208089, New Haven, CT 06520-8089 (e-mail: alan.dardik@yale.edu).

The editors and reviewers of this article have no relevant financial relationships to disclose per the JVS-Vascular Science policy that requires reviewers to decline review of any manuscript for which they may have a conflict of interest.

2666-3503

https://doi.org/10.1016/j.jvssci.2021.05.002

An arteriovenous fistula (AVF) is a surgical shunt most commonly created to serve as an access for hemodialysis. AVF supply the high flow rates necessary for patients with end-stage renal disease (ESRD) to receive adequate and efficient hemodialysis.[1,2] A recent multicenter study in the United States found that the median AVF flow rate 6 weeks after upper arm AVF creation was 1050 mL/min.[3] These high flow rates, which represent a significant fraction of cardiac output, impose a significant additional burden on the heart that is suspected to result in significant cardiovascular effects that may be especially detrimental in patients with ESRD. Longitudinal cardiac imaging of human patients has documented long-term structural cardiac changes after AVF placement,[4-9] with many changes including left ventricular (LV) hypertrophy,[4-7,9] as well as both atrial[6,7] and right ventricular[7,8] enlargement. It is often assumed that these AVF-induced structural changes to the heart are deleterious, because LV hypertrophy is a potent risk factor for adverse cardiovascular end points such as stroke, coronary disease, and heart failure.[10] However, cardiac hypertrophy is not always maladaptive; for example, endurance athletes and pregnant women also have enlarged hearts in response to prolonged elevations in cardiac output. In these cases, adaptive or physiologic cardiac hypertrophy is thought to be benign if not potentially beneficial to cardiovascular health.[11,12] Unfortunately, it is not clear whether AVF-induced cardiac hypertrophy is adaptive or maladaptive in patients with ESRD on hemodialysis.

A recent clinical trial showed that ligation of the AVF after renal transplantation resulted in significant decreases in LV mass, LV and left atrial volumes, and N-terminal pro-brain natriuretic peptide, suggesting the reversibility of the cardiac adaptive remodeling.[13] In addition, AVF can have positive cardiovascular effects, such as amelioration of hypertension,[14] leading to the placement of percutaneous ilioiliac AVF in patients with medically refractory hypertension.[15-17] Prior observational clinical studies have also suggested a benefit of AVF to cardiovascular health, showing that patients with ESRD and AVF have fewer cardiovascular events and lower cardiovascular-specific mortality compared with patients with central venous catheters, despite the inherent limitations owing to their retrospective design.[18-20] These human studies suggest the possibility that the structural cardiac changes associated with AVF are adaptive, reversible, and potentially beneficial.

We have previously shown that the mouse aortocaval fistula model recapitulates many features of human AVF maturation.[21,22] In contradistinction to other aortocaval fistulae mouse models where heart failure is intentionally induced with large diameter fistulae and is associated with high perioperative mortality,[23,24] our model uses a smaller diameter fistula that is well-tolerated.[21,25] Using this model, we characterize the structural, functional, and molecular features of AVF-induced cardiac remodeling; we hypothesized that the cardiac hypertrophy induced by the AVF is associated with cardioprotective molecular features.

ARTICLE HIGHLIGHTS

- **Type of Research:** Basic science study
- **Key Findings:** Murine arteriovenous fistulae stimulate cardiac hypertrophy without causing systolic dysfunction, diastolic dysfunction, pathologic fibrosis, or heart failure. Left ventricle transcriptomics suggests activation of proangiogenic, prosurvival, and procardiogenic factors in addition to electrical remodeling with a downregulation of several ion channels.
- **Take Home Message:** Arteriovenous fistulae stimulate adaptive cardiac hypertrophy that is associated with cardioprotective, but also arrhythmogenic, transcriptomic features.

METHODS

Animals and surgery. All animal work was compliant with, and approved by, the Yale Animal Care and Use Committee and in accordance with all provisions of the Public Health Service Policy on Humane Care and Use of Laboratory Animals (NIH assurance: D16-00146 [A3230-01]). Male and female C57Bl/6 mice between 9 and 11 weeks of age were treated with sham laparotomy or AVF creation via puncture of the infrarenal aorta into the vena cava with a 25G needle as described previously.[21,26] Briefly, animals were anesthetized with 2% to 3% inhaled isoflurane, and a midline laparotomy was made, and the bowels related superolaterally to expose the aorta and vena cava. The suprarenal aorta and vena cava were clamped, and the infrarenal aortocaval fistula subsequently created with puncture by a 25G needle (Fig 1, *A*). The arteriotomy was covered with retroperitoneum and hemostasis achieved with gentle pressure. AVF patency was confirmed intraoperatively by visualizing pulsatile distension of the IVC with bright oxygenated blood, and also postoperatively by serial transabdominal pulse-wave Doppler imaging (Fig 1, *B*). Animals received 0.1 mg/kg buprenorphine intraperitoneally twice daily postoperatively for 2 days for pain control.

Echocardiography. Transthoracic echocardiography was performed on sham (male, n = 5; female, n = 3) and AVF (male, n = 6, female, n = 3) mice at 5 weeks postoperatively. Studies were performed under isoflurane anesthesia (1%-2%) while maintaining physiological conditions with a heated imaging stage using a high resolution ultrasound imaging system (Vevo 2100, FUJIFILM VisualSonics Inc, Toronta, Calif). Two-dimensional B-mode and M-mode images were obtained with a 40-MHz

transducer in both standard parasternal short axis and long axis views for determination of the LV ejection fraction, end-diastolic dimensions, cardiac output, anterior wall thickness and posterior wall thickness. The relative wall thickness was defined as the average wall thickness (anterior wall thickness/2 + posterior wall thickness/2) divided by the LV end-diastolic volume. LV diastolic function was estimated using mitral E/E′, as determined by pulsed wave Doppler at the level of the mitral valve tips and tissue Doppler of the medial and lateral mitral valve annulus in the apical four chamber view. Right heart indices were estimated using mean pulmonary artery pressures and tricuspid annular plane systolic excursion (TAPSE). The mean pulmonary artery pressure was calculated from the pulmonary acceleration time and pulmonary ejection time, obtained by placing the pulsed wave Doppler cursor in the right ventricular outflow tract just proximal to the pulmonary valve leaflets in the parasternal short axis view. TAPSE was obtained by measuring the highest and lowest points of the tissue Doppler signal obtained along the lateral part of the tricuspid valve in the apical four chamber view.

Cardiac computed tomography angiography. Cardiac computed tomography (CT) was performed on postoperative week 5 on sham (male, n = 3, female, n = 2) and AVF (male, n = 3, female, n = 2) mice. Approximately 100 μL of a nanoparticulate contrast agent, ExiTron nano 12000 (Miltenyi Biotech, Bergisch Gladbach, Germany), was injected via tail vein. Animals were then placed prone on a horizontal stage under light anesthesia (1% isoflurane), and images obtained using a micro-CT scanner (MicroSPECT4CT; MILabs, Houten, the Netherlands) using retrospective cardiac and respiratory gating, with a cone beam filtered back projection algorithm set to 40 μm effective voxel size. Micro-CT was performed with a 50-kVp x-ray tube voltage, 430-uA tube current, 20 milliseconds per frame, 360° angle, and 0.75° increments per view. Cardiac chambers were manually segmented and volumes quantified using 3DSlicer (www.slicer.org).

Histology. Hearts from sham (male, n = 3, female, n = 3) and AVF (male, n = 4, female, n = 3) mice were excised at postoperative week 5, rinsed with normal saline solution, and immersed in 10% neutralized buffered formalin for 24 to 48 hours. The tissue block was then embedded in paraffin and cut in 5-μm cross-sections. Masson's trichrome staining was used to assess collagen content and identify areas of fibrosis at both low and high magnification. Quantification of collagen area fraction was performed in high-powered (400×) coronal sections for each of the four cardiac chambers, using automated color segmentation by isolating blue pixels coloring collagen using Matlab (MathWorks, Natick, Mass). The cardiomyocyte surface area was quantified in the same high-powered coronal sections by taking the average of at least 10 myocyte cross-sectional areas per chamber per section measured via manual polygonal segmentation using ImageJ (NIH, Bethesda, Md).

RNA extraction and RNA sequencing. Left ventricles were harvested from sham (male, n = 3; female, n = 3) and AVF (male, n = 3; female, n = 3) mice at postoperative day 10, and flash frozen with liquid nitrogen and stored at −80°C. Total RNA was then isolated using RNeasy Mini Kit with digested DNase I (Qiagen; Valencia, Calif). RNA quality and concentration were measured using a NanoDrop spectrophotometer (Thermo Scientific; Wilmington, Del), and by electropherogram (Agilent 2100 Bioanalyzer, Santa Clara, Calif). RNA sequencing was performed by the Yale Center for Genome Analysis, where messenger RNA (mRNA) library was prepared using KAPA Stranded mRNA-Seq Kit (Roche, Basel, Switzerland), and next generation sequencing performed with NovaSeq 6000 (Illumina, San Diego, Calif).

RNA sequencing data analysis. Raw sequencing reads were imported into Partek Flow servers (Partek, Chesterfield, Mo), where reads were aligned to the NIH-GRCm38.p6 genome using HISAT2 (v2.1.0) and annotated with Partek E/M on annotation model (NIH-R106). Differential gene expression was carried out with DESeq2 (v3.5). Significantly differentially expressed genes (false discovery rate of <0.05, absolute fold change of >1.5) were imported into Ingenuity Pathway Analysis (Qiagen, Hilden, Germany) for determination of activated or inactivated signaling pathways, upstream regulators, and downstream effects.

Statistical analysis. Data are represented as mean ± standard error of the mean. Unless otherwise specified, data was analyzed using Prism 8 software (GraphPad, La Jolla, Calif). *P* values of less than .05 were considered statistically significant.

RESULTS

AVF induces cardiac hypertrophy without disrupting cardiac function. For this study, AVF were created in 60 mice (32 male, 28 female) with an overall survival rate of 83% and patency rate of 63% (Fig 1, *C*). All technical deaths occurred within 48 hours of surgery (4 male, 6 female). AVF creation resulted in progressive dilatation of the infrarenal inferior vena cava and aorta, consistent with maturation of the AVF (Fig 1, *D-F*) as previously reported.[21,22] At the terminal time point of 5 weeks postoperatively, cardiac hypertrophy was visible in mice with AVF (Fig 2, *A*), corresponding with a 144% increase in normalized heart weights (Fig 2, *B*). Normalized lung weights (Fig 2, *C*) and total body weights (Fig 2, *D*) remained unchanged between sham and AVF. Cardiac computed tomography angiography (Fig 2, *E* and *F*) was performed on a subset of mice to assess for structural cardiac changes and demonstrated that all four chambers were enlarged significantly

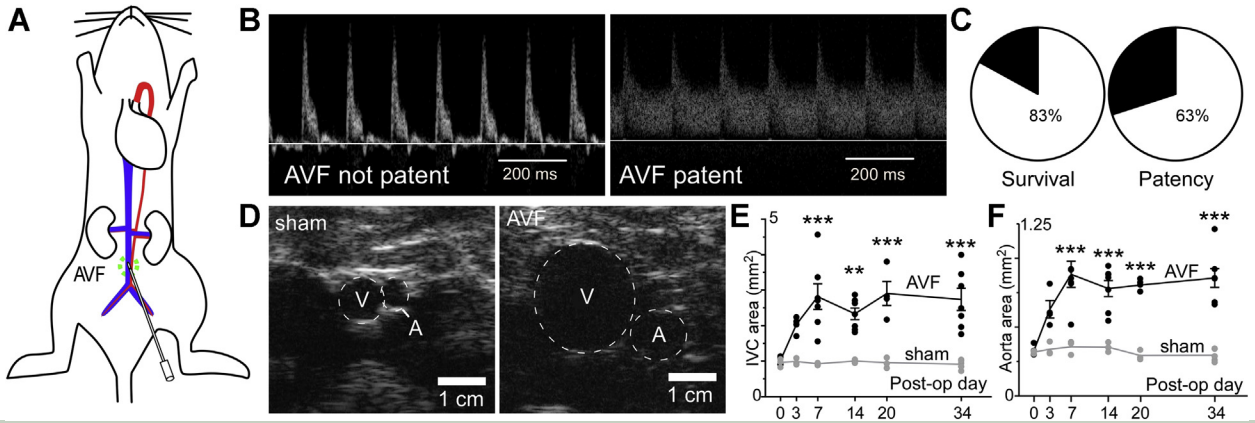

Fig 1. Mouse model of arteriovenous fistulae (*AVF*). **A,** Schematic of infrarenal aortocaval fistula created by needle puncture with a 25G needle. **B,** Doppler waveforms of the proximal infrarenal aorta distinguishes a nonpatent AVF with high resistance flow (*left*) from a patent AVF with low resistance flow (*right*). **C,** The overall survival was 83% and patency was 63% (n = 60 mice). **D,** Exemplar axial two-dimensional ultrasound images from the proximal infrarenal aorta and inferior vena cava (*IVC*) of the sham and AVF mice at postoperative week 5. **E-F,** Quantitation of cross-sectional infrarenal IVC and aorta area after surgery shows progressive IVC dilation after AVF; sham: n = 3-6; AVF: n = 4-7; ** $P < .01$, ***$P < .001$, 2-way repeated measures analysis of variance with Sidak's post hoc test.

after AVF when compared with sham (Fig 2, *F*). Cardiac echocardiography was performed to further define serial changes in cardiac structure and function after AVF (Fig 2, *G-O*). Compared with sham mice, we found that AVF resulted in a 131% increase in weight-normalized LV end-diastolic volume (Fig 2, *H*), and a 23% decrement in LV end-diastolic volume normalized wall thickness (Fig 2, *I*). Weight-normalized left atrial area was 124% larger with AVF compared with sham mice (Fig 2, *J*). With regard to LV function, the weight-normalized cardiac output was 147% larger in AVF mice relative to sham mice (Fig 2, *K*), although the LV ejection fraction (Fig 2, *L*) and mitral E/E' (Fig 2, *M*), as well as the index of diastolic function, were not significantly different. Similarly, indices of right ventricular function such as mean pulmonary artery pressure (Fig 2, *N*) and TAPSE (Fig 2, *O*) were not different between AVF and sham mice. Neither valvular regurgitation nor stenosis was seen in any animal at 5 weeks postoperatively. Analyzing these data stratified by sex did not reveal significant sex-dependent differences, with both sexes demonstrating significant increases in normalized heart weight, cardiac output, and chamber volumes without changing systolic or diastolic function (Supplementary Fig 1). Thus, AVF resulted in cardiac structural changes without significantly affecting cardiac function.

AVF-induced cardiac hypertrophy does not cause fibrosis or alter collagen content. We next determined whether cardiac hypertrophy triggered by AVF might cause cardiac fibrosis or resulted in ECM loss. Cardiac sections from both sham and AVF groups at 5 weeks postoperative were stained with Masson's trichrome, which colors collagen and areas of fibrosis blue. Examination of these cardiac sections at both low magnification (Fig 3, *A* and *B*) or at high magnification (Fig 3, *C-F*) show that AVF-induced cardiac hypertrophy is not accompanied by any patchy or perivascular fibrosis in any of the four cardiac chambers. Furthermore, quantification of interstitial collagen showed that there was no appreciable change in the collagen area fraction in any of the four chambers (Fig 3, *G-J*). Stratifying by sex, there was a trend toward decreased interstitial collagen in female mice, although this difference did not reach statistical significance (Supplementary Fig 1, *M*). Similarly, the quantification of collagen using picrosirius red staining on cardiac sections showed absence of patchy fibrosis and no significant change in collagen content in all four cardiac chambers with AVF compared with sham (Supplementary Fig 2). Finally, compared with sham, cardiomyocyte surface area (normalized by body weight) was enlarged with AVF in the left ventricle, left atrium, and right ventricle, consistent with cellular hypertrophy (Fig 3, *K-M*). There was a trend toward cardiomyocytes being larger in the right atrium as well, but this result did not reach statistical significance (Fig 3, *N*).

Transcriptomics of AVF-induced cardiac hypertrophy suggests potential benefits and risks. Because these data show that an AVF stimulates cardiac hypertrophy without any overt signs of harm, we next determined the molecular profile of the hypertrophic response to examine both the biological basis of AVF-stimulated LV hypertrophy as well as to use molecular bioinformatics to predict possible AVF-stimulated physiological responses. Therefore, we performed RNA sequencing of mRNA isolated from the left ventricles of mice 10 days after AVF or sham laparotomy; this time point was chosen to reflect the molecular signatures of the evolving LV

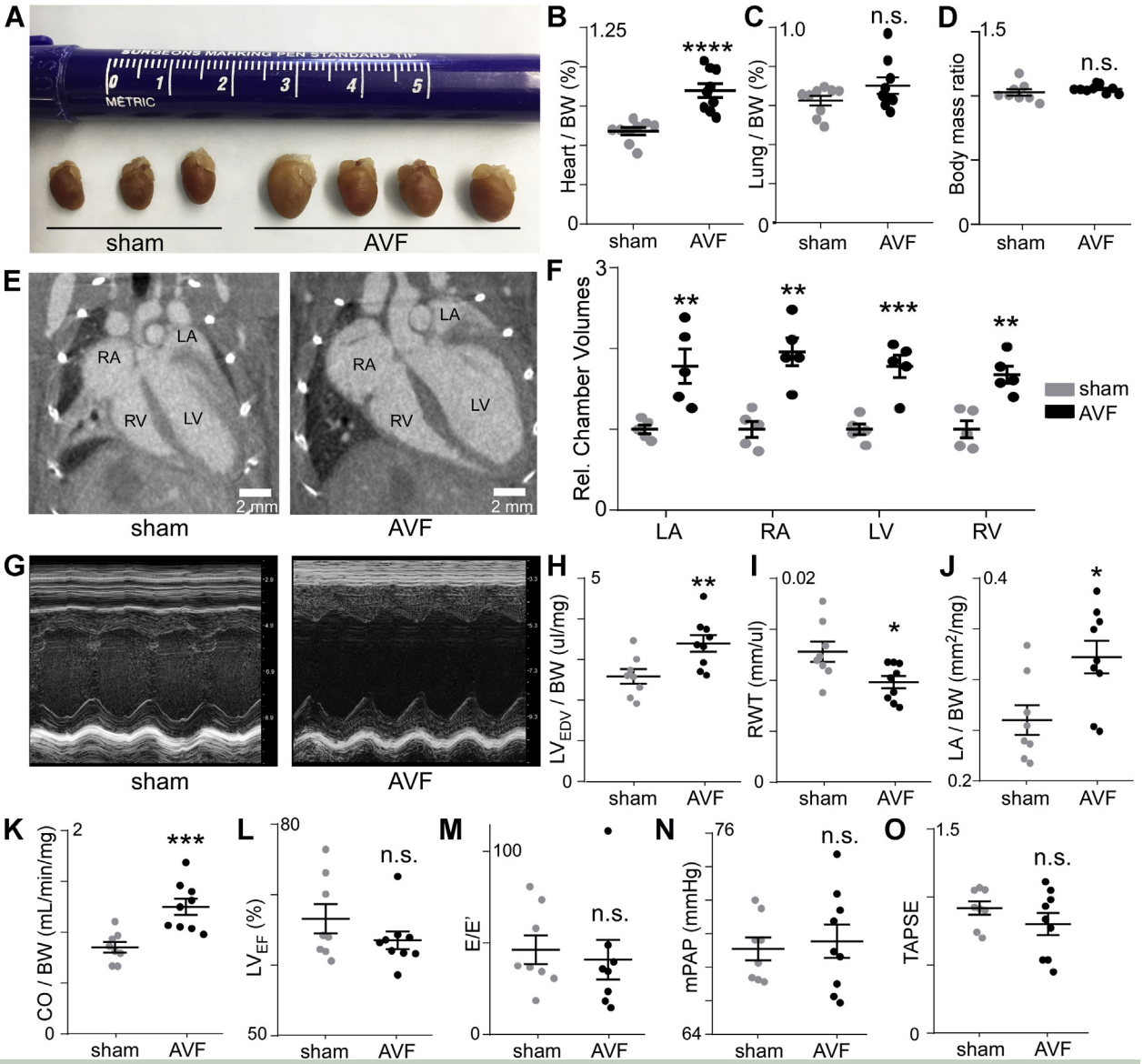

Fig 2. Arteriovenous fistulae (*AVF*) induce cardiac hypertrophy without disrupting cardiac function. **A,** Exemplar images of excised sham and AVF hearts at postoperative week 5 showing enlarged hearts after AVF. **B,** Heart mass normalized to body weights at postoperative week 5 confirm AVF-induced cardiac hypertrophy (n = 9 each, unpaired *t* test). **C,** Normalized lung masses exhibited no significant change between sham and AVF at post-operative week 5 (n = 9 each; unpaired *t* test). **D,** No significant difference in the fold-change in body mass at postoperative week 5 relative to baseline between sham and AVF mice (n = 8-9 each; unpaired *t* test). **E,** Exemplar two-dimensional four-chamber view of cardiac computed tomography angiography (CTA) from sham and AVF mice at postoperative week 5. **F,** Quantitation of CTA volumes showed significant enlargement of all four cardiac chambers after AVF when compared with sham (n = 5 each; unpaired *t* test). **G,** Exemplar mid-cavity short axis M-mode echo images from LV of sham and AVF mice at postoperative week 5. **H-O,** Summary echocardiographic indices of cardiac structure and function after AVF or sham surgery at postoperative week 5 (n = 8-9 each; unpaired *t* test). *CO/BW,* Cardiac output normalized to body weight; *E/E',* index of diastolic function; *LA,* left atrium; *LV,* left ventricle; LV_{EDV}, LV end-diastolic volume; LV_{EF}, left ventricular ejection fraction; *RWT,* relative wall thickness; *LA/BW,* left atrial area normalized to body weight; *mPAP,* mean pulmonary artery pressure; *RA,* right atrium; *RV,* right ventricle; *TAPSE,* tricuspid annular plane systolic excursion; * $P < .05$, ** $P < .01$, *** $P < .001$.

hypertrophy while minimizing any nonspecific acute stress response from the initial surgery. We obtained an average of 53 million reads (range, 43.8-65.8 million reads) per sample, of which 96.4% (range, 94.5%-97.9%) were aligned to the reference C57Bl/6 mouse genome (GRCm38.p6) using HISAT2. We then quantified the number of genes represented and compared using DEseq2 which genes were significantly differentially

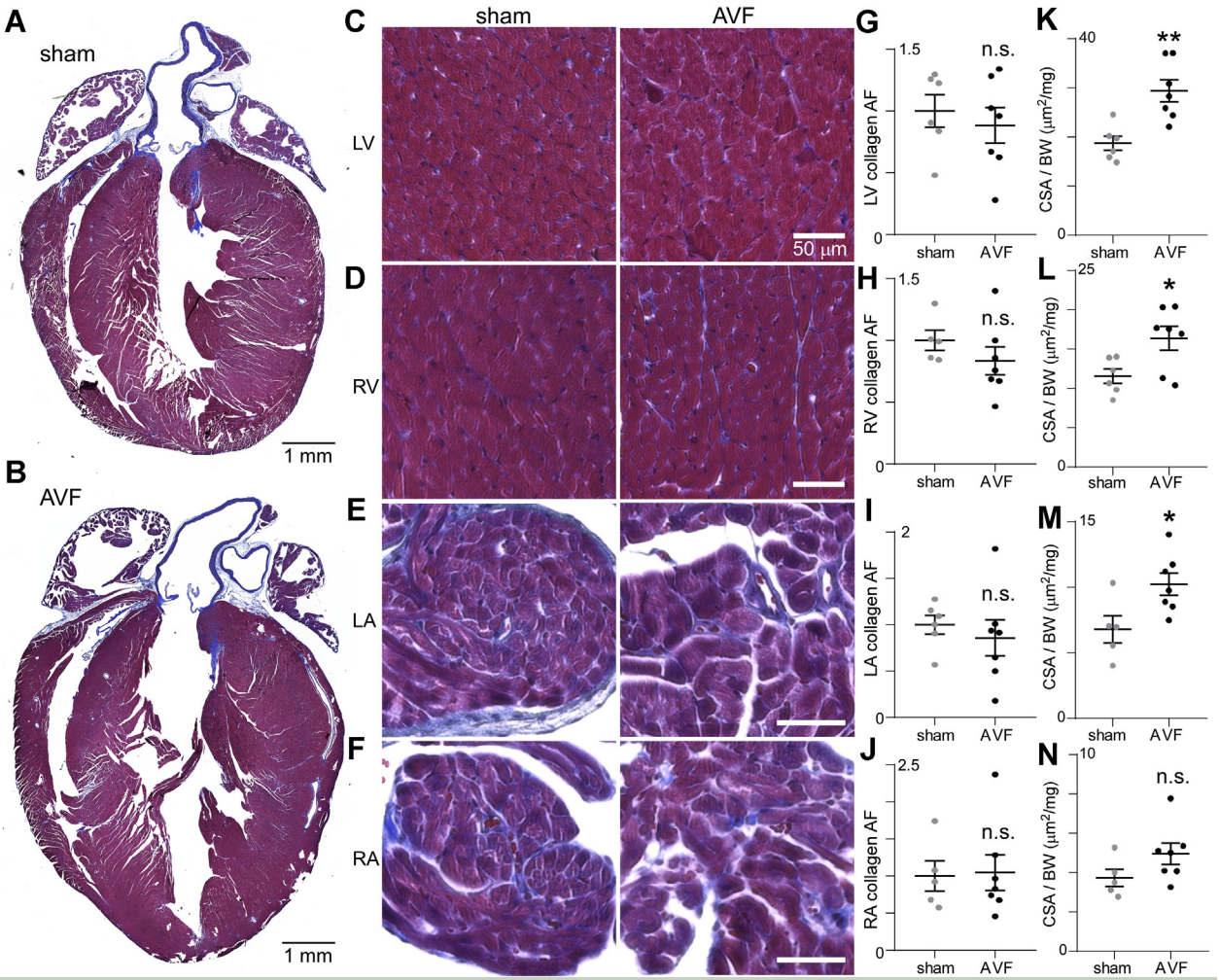

Fig 3. Arteriovenous fistulae (*AVF*)-induced cardiac hypertrophy does not cause fibrosis or alter collagen content. **A-B,** Exemplar low-magnification four-chamber coronal cardiac sections stained with Masson's trichrome after sham **(A)** or AVF **(B)** surgery showing absence of patchy fibrosis. **C-F,** Exemplar high-magnification views from left ventricle (*LV*), right ventricle (*RV*), left atrium (*LA*), and right atrium (*RA*) of sham (*left*) and AVF (*right*) mice. **G-J,** Summary data showing no significant change in collagen area fraction (AF) in any of the four cardiac chambers between sham (n = 5-6) and AVF (n = 7) animals (unpaired *t* test). **K-N,** Summary data showing increased cardiomyocyte cross-sectional area (*CSA*), normalized to body weight (*BW*) with AVF compared with sham (unpaired *t* test). * $P < .05$, ** $P < .01$, n.s. $P > .05$.

expressed between AVF and sham mice. Of the 19 384 genes for which transcripts were detected, 857 genes were significantly different (false discovery rate of <0.05, with at least a fold change of ±1.5; colored blue and orange in Fig 4, *A*; Appendix 2).

We first examined genes expected to be regulated in cardiac hypertrophy, such as fetal genes, and genes implicated in cardiac metabolism and extracellular matrix (ECM) expression (Fig 4, *B*). Several fetal cardiac genes governed by NFAT, MEF2, and GATA4 were differentially expressed, including the upregulation of Nppa, Nppb, Rcan1, Acta1, Myl1, Ankrd1, and Meox1, and the downregulation of Atp2a2 and Myh6. Ppara, an important regulator of fatty acid metabolism in the heart, was slightly downregulated. Transcripts of multiple ECM-related proteins, including multiple subunits of collagen, collagen processing molecules, filaments, and matricellular proteins, as well as proteoglycans and glycoproteins were all upregulated with the exception of Lama5. Unexpectedly, several ion channels, including the sodium, potassium, and calcium channels, were downregulated. These trends were similar in both male and female mice (Supplementary Table). We validated a selection of our results with quantitative real-time polymerase chain reaction and found a good correlation between quantitative real-time polymerase chain reaction and RNA sequencing ($R^2 = 0.84$; Supplementary Fig 3).

We next took an unbiased approach to identify important signaling molecules implicated in AVF-induced LV hypertrophy. We used Qiagen's Ingenuity Pathway

A

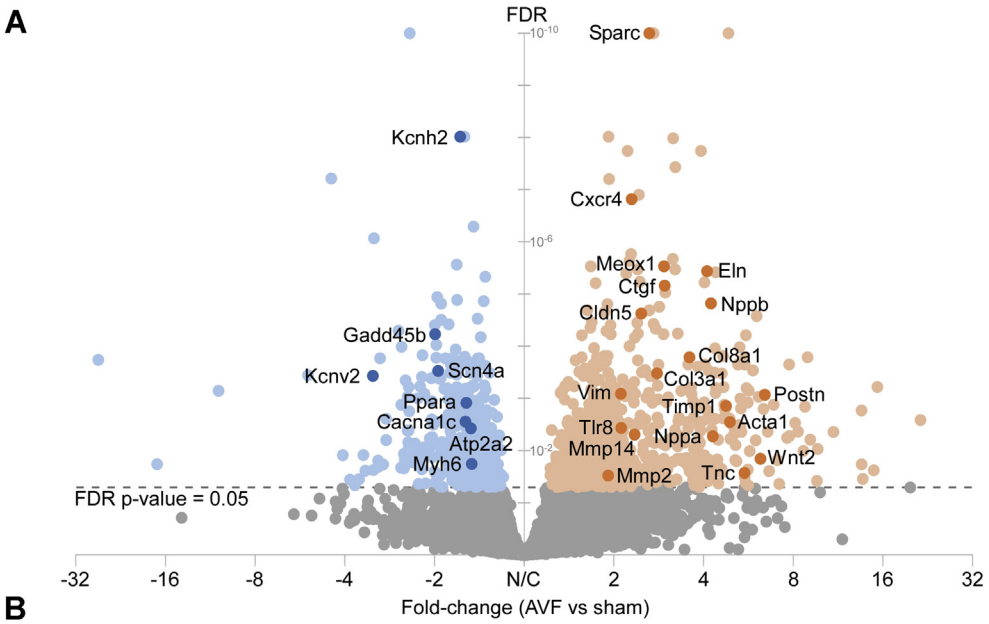

B

Gene	Counts	p	FDR	Fold-change	Gene	Counts	p	FDR	Fold-change
Cardiac Fetal Genes									
NFAT-related					GATA4-related				
Nppa	193344	1.46E-04	5.34E-03	4.30	Ankrd1	761693	1.49E-05	1.05E-03	2.82
Nppb	147908	3.68E-08	1.51E-05	4.24	Meox1	18135	4.23E-09	2.96E-06	2.95
Rcan1	62486	4.58E-04	1.17E-02	2.02	Myh6	7885234	8.81E-04	1.80E-02	-1.50
					Myl1	15362	1.48E-03	2.57E-02	1.65
MEF2-related					Nppa	193344	1.46E-04	5.34E-03	4.30
Acta1	618625	5.92E-05	2.85E-03	4.90	Nppb	147908	3.68E-08	1.51E-05	4.24
Atp2a2	6158932	9.10E-05	3.78E-03	-1.51					
Myh6	7885234	8.81E-04	1.80E-02	-1.50					
Metabolism									
Ppara	48433	1.90E-05	1.22E-03	-1.56					
Ion Channels									
Cacna1c	109893	5.76E-05	2.80E-03	-1.57	Kcnv2	4509	3.38E-06	3.72E-04	-3.22
Kcnh2	43015	3.79E-12	9.64E-09	-1.64	Scn4a	20865	2.30E-06	2.98E-04	-1.94
Extracellular Matrix									
Collagen-related					Other structural				
Col1a1	99450	9.38E-04	1.86E-02	2.37	Acta1	618625	5.92E-05	2.85E-03	4.90
Col1a2	99361	1.05E-03	2.02E-02	2.29	Eln	33711	6.08E-09	3.65E-06	4.11
Col3a1	221176	2.89E-06	3.32E-04	2.79	Vim	176208	1.05E-05	8.22E-04	2.11
Col4a1	445630	8.74E-04	1.80E-02	2.33					
Col4a3	3257	1.28E-05	9.57E-04	3.04	Matricellular proteins				
Col5a1	42004	1.17E-03	2.18E-02	2.15	Ctgf	37603	1.46E-08	6.92E-06	2.96
Col5a2	27923	8.54E-06	7.17E-04	3.36	Fbln2	51731	2.95E-03	4.06E-02	1.90
Col5a3	17413	4.08E-04	1.07E-02	2.50	Postn	85604	1.11E-05	8.54E-04	6.42
Col6a1	55200	1.88E-03	3.02E-02	1.91	Sparc	400331	1.82E-14	7.11E-11	2.63
Col6a2	63424	2.71E-03	3.85E-02	1.92	Tnc	3669	1.59E-03	2.68E-02	5.49
Col8a1	28205	8.67E-07	1.64E-04	3.59					
Col12a1	1950	1.59E-04	5.73E-03	7.63	Proteoglycans and Glycoproteins				
Col14a1	13693	5.93E-06	5.72E-04	2.81	Bgn	172483	2.20E-04	7.06E-03	2.15
Col15a1	88312	6.41E-04	1.47E-02	2.20	Cd44	7167	6.79E-06	6.10E-04	1.88
Col16a1	5750	7.49E-04	1.62E-02	2.85	Fbn1	66996	1.65E-06	2.28E-04	2.82
Col18a1	15707	1.49E-03	2.57E-02	2.55	Fn1	52405	2.36E-04	7.39E-03	2.91
Col26a1	641	5.71E-04	1.37E-02	3.89	Lama5	58734	2.11E-05	1.33E-03	-1.66
Lox	4856	8.10E-04	1.69E-02	2.91	Lum	27722	5.93E-05	2.85E-03	1.88
Mmp2	33164	1.78E-03	2.92E-02	1.92	Vcan	10638	2.01E-04	6.62E-03	2.63
Mmp14	18591	1.32E-04	4.97E-03	2.35					
Mmp23	3474	7.51E-04	1.62E-02	1.98					
Timp1	2088	2.28E-05	1.40E-03	4.76					

Fig 4. Transcriptomics of arteriovenous fistulae (AVF)-induced left ventricular (LV) hypertrophy. **A,** Volcano plot of 19 384 genes, of which 223 were significantly downregulated, and 634 were significantly upregulated (false discovery rate [*FDR*] of <0.05, and |fold change| of >1.5). Messenger RNA from LV at postoperative day 10 (n = 6 each), annotated and aligned with HISAT2 and differential expression analysis with DEseq2. Genes with suspected or known roles in cardiac hypertrophy are highlighted. **B,** Tabulation of selected significantly differentially expressed genes from cardiac fetal genes, metabolism, ion channels, and extracellular matrix (ECM).

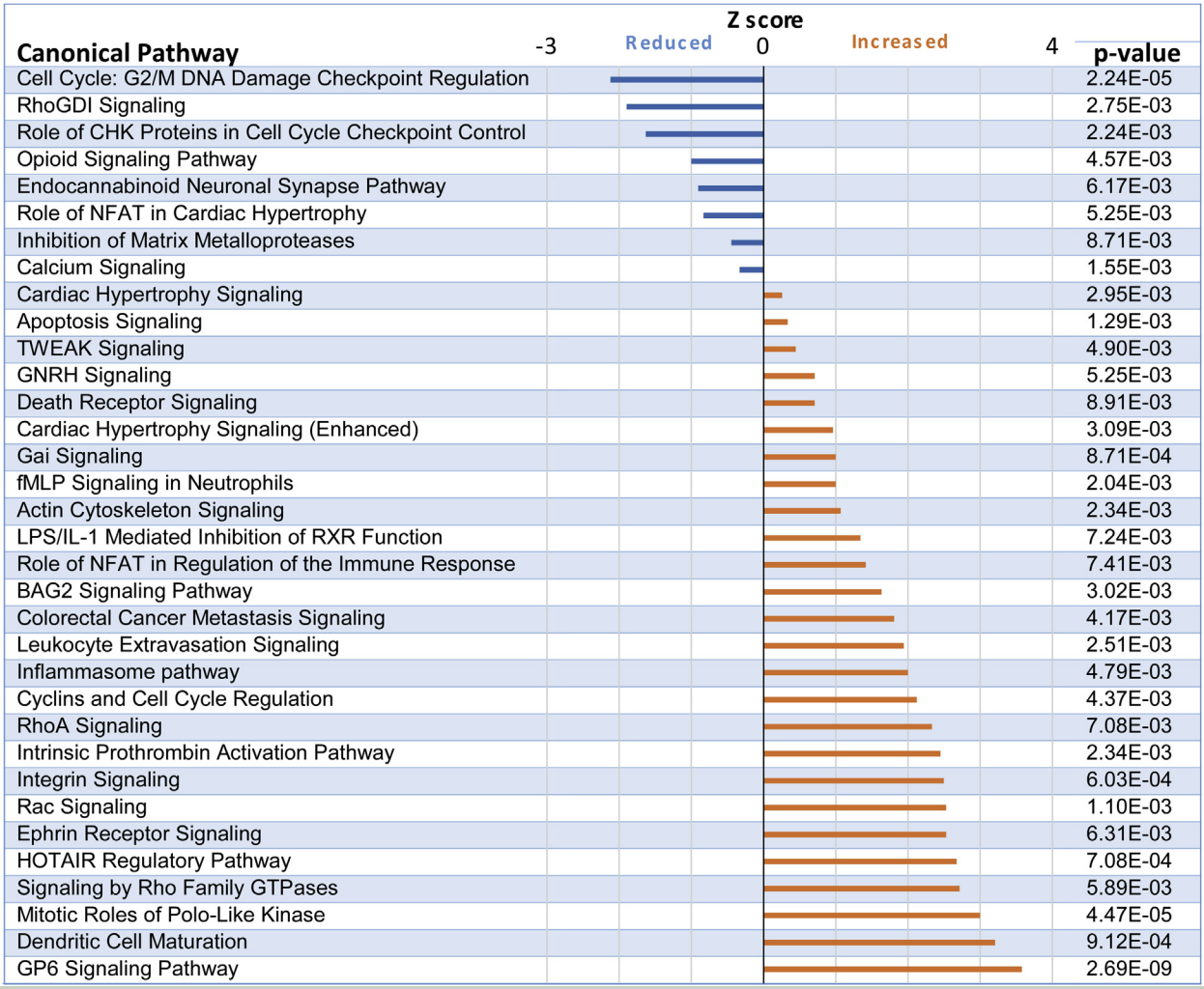

Fig 5. Predicted top activated or inactivated canonical pathways by arteriovenous fistulae (AVF)-induced left ventricular (LV) hypertrophy.

Analysis to compare all significantly differentially expressed genes with its curated database of signaling networks to predict which canonical signaling pathways are activated (Z-score of >0) or inactivated (Z-score of <0) after AVF. The top 34 canonical pathways with the lowest *P* values and nonzero Z-scores are shown in Fig 5. Predictably, canonical pathways for cardiac hypertrophy signaling and cardiac hypertrophy signaling (enhanced) were activated. Of interest, NFAT-mediated cardiac hypertrophy, a well-known trigger of pathologic cardiac hypertrophy,[27] was predicted to be inactivated. Other pathways represented included cell cycle-related signaling, inflammation-related signaling, and ECM-related signaling, among others.

We next identified upstream regulators of AVF-induced LV hypertrophy. The top 30 most statistically significant activated or inactivated regulators, with absolute Z-scores of greater than 2, are shown in Fig 6 and include multiple molecules previously implicated in a variety of cardiovascular diseases. As expected, many of these regulators predicted to be upregulated are genes previously implicated in cardiac hypertrophy such as Akt1,[28,29] androgen receptor,[30] Mitf,[31,32] Mtpn,[33] and Tgfb1,[34,35] as well as well-known mediators of inflammation such as Ccr2,[36] Csf2,[37] Ifng,[38] Ige,[39,40] IL-4,[41-43] IL-6,[42] and TNF.[44] In addition, other regulators predicted to be activated include molecules that support or increase cardiogenesis such as Akt1,[45,46] Ccnd1,[47] Erbb2,[48] Foxm1,[49-51] and Hgf.[52,53] Similarly, negative regulators of cardiogenesis such as alpha-catenin,[54] Cdkn1A,[55,56] and Foxo3,[57,58] were predicted to be repressed. Interestingly, let-7 and mir-21, which are microRNAs with complex pleotropic roles but had previously been reported to increase cardiogenesis,[59-66] were predicted to be downregulated with AVF. Molecules that increase angiogenesis such as Vegf,[67] Akt1,[45,46,68] Erbb2,[69] and Hgf,[70,71] were predicted to be activated. Furthermore, molecules that were cardioprotective in animal models of cardiovascular disease such as Akt1,[72] Areg,[73] and Hgf,[71,74,75] were predicted to be activated, although excessive activation of Akt1 and Areg have also been reported to worsen cardiac

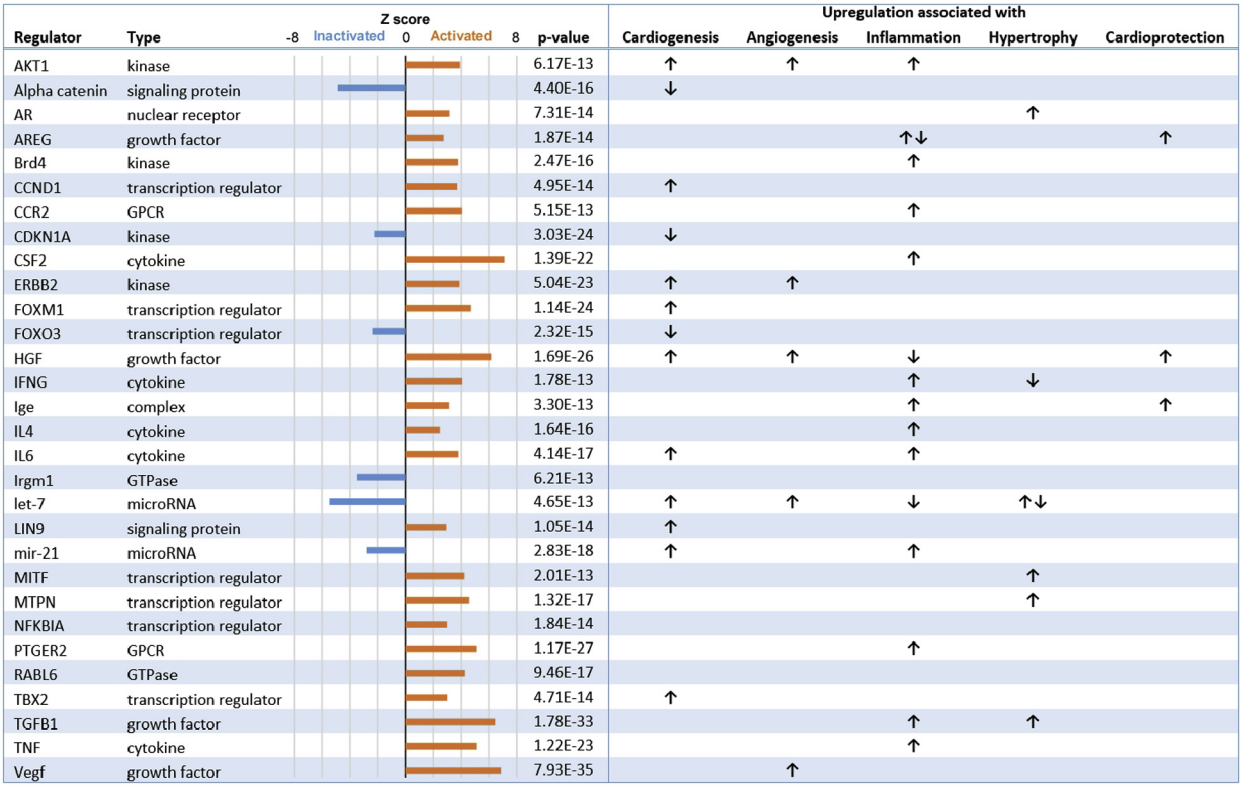

Regulator	Type	p-value	Upregulation associated with: Cardiogenesis	Angiogenesis	Inflammation	Hypertrophy	Cardioprotection
AKT1	kinase	6.17E-13	↑	↑	↑		
Alpha catenin	signaling protein	4.40E-16	↓				
AR	nuclear receptor	7.31E-14				↑	
AREG	growth factor	1.87E-14			↑↓		↑
Brd4	kinase	2.47E-16			↑		
CCND1	transcription regulator	4.95E-14	↑				
CCR2	GPCR	5.15E-13			↑		
CDKN1A	kinase	3.03E-24	↓				
CSF2	cytokine	1.39E-22			↑		
ERBB2	kinase	5.04E-23	↑	↑			
FOXM1	transcription regulator	1.14E-24	↑				
FOXO3	transcription regulator	2.32E-15	↓				
HGF	growth factor	1.69E-26	↑	↑	↓		↑
IFNG	cytokine	1.78E-13			↑	↓	
Ige	complex	3.30E-13			↑		↑
IL4	cytokine	1.64E-16			↑		
IL6	cytokine	4.14E-17	↑		↑		
Irgm1	GTPase	6.21E-13					
let-7	microRNA	4.65E-13	↑	↑	↓	↑↓	
LIN9	signaling protein	1.05E-14	↑				
mir-21	microRNA	2.83E-18	↑		↑		
MITF	transcription regulator	2.01E-13				↑	
MTPN	transcription regulator	1.32E-17				↑	
NFKBIA	transcription regulator	1.84E-14					
PTGER2	GPCR	1.17E-27			↑		
RABL6	GTPase	9.46E-17					
TBX2	transcription regulator	4.71E-14	↑				
TGFB1	growth factor	1.78E-33			↑	↑	
TNF	cytokine	1.22E-23			↑		
Vegf	growth factor	7.93E-35		↑			

Fig 6. Predicted top upstream regulators of arteriovenous fistulae (AVF)-induced left ventricular (LV) hypertrophy (left), with their reported roles in cardiogenesis, angiogenesis, inflammation, hypertrophy and cardioprotection in the literature (*right*).

dysfunction.[76,77] There were no significant sex-specific differences in the pattern of regulator function (Supplementary Fig 4).

Using a bioinformatic approach, we determined whether the transcriptomics of AVF-induced LV hypertrophy would affect cardiovascular-specific diseases or biological processes. These data show that the dataset genes suggest an increase in cardiogenesis, vasculogenesis, and angiogenesis (Fig 7). The data also predict increased endothelial cell adhesion, as would be expected from increased inflammation. Interestingly, pathway analysis predicted increased risk of arrhythmia, likely owing to alterations in ion channel expression. Finally, there was also a predicted decrease in the risk of cardiac damage, suggesting a cardioprotective feature of AVF-induced cardiac remodeling.

DISCUSSION

We show in both male and female wild-type mice that an aortocaval fistula triggers a high output state, inducing adaptive cardiac hypertrophy with preserved cardiac function and without heart failure. This AVF-induced cardiac remodeling occurs without fibrosis or loss of collagen content and has transcriptomic signatures that are associated with increased arrhythmogenicity, cardiogenesis, and angiogenesis. These data show that the cardiac adaptation to an AVF is accompanied by molecular features that suggest both cardioprotection and potential cardiac risk.

Our work is different from prior research investigating the effects of volume overload on cardiac remodeling because we used an AVF of smaller diameter. For instance, Scheuermann-Freestone et al,[23] who were among the first to establish the mouse aortocaval fistula heart failure model, used needles with an 0.6 mm outer diameter (approximately 23G); in their experience, male mice had an unacceptably high mortality so only female mice were used, with a 42% perioperative mortality and impaired LV contractility at 4 weeks postoperatively.[23] In contrast, we used 25G needles (outer diameter of 0.5 mm) that resulted in a lower perioperative mortality of 17% (males vs females, 12% vs 21%, respectively; $P = .56$), and without producing clinical signs of heart failure (Fig 2, *C* and *D*) or affecting the LV ejection fraction (Fig 2, *L*). This finding is consistent with our own previous experience using smaller needles (25G or 28G) for aortocaval fistula creation that were associated with increased survival but decreased AVF patency.[25] Nevertheless, our results were similar in other respects; we showed that animals with AVF had eccentric hypertrophy with increased LV mass, increased LV end-diastolic volume, and decreased relative wall thickness.[23,24,78] In addition, there was preserved LV ejection fraction, LV diastolic function

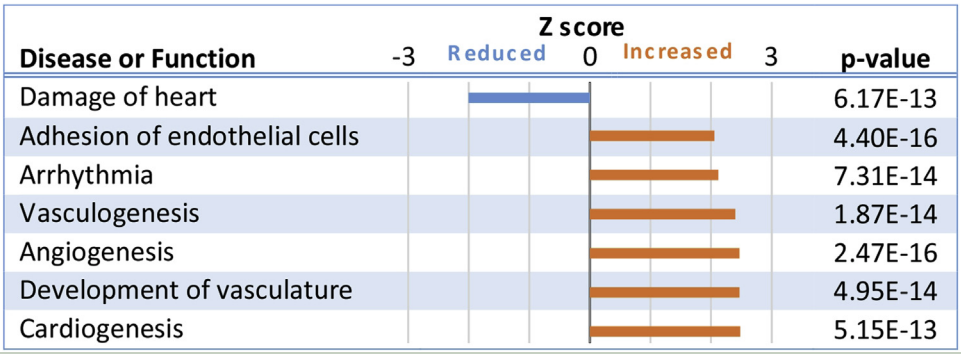

Fig 7. Predicted downstream effects of arteriovenous fistulae (AVF)-induced left ventricular (LV) hypertrophy.

as estimated by mitral E/E' (Fig 2, *M*), and indices of right heart function such as the mean pulmonary artery pressure (Fig 2, *N*) and TAPSE (Fig 2, *O*). Importantly, we did not find significant sex-dependent differences in the cardiac adaptation to AVF (Supplementary Fig 1). These findings, together with a well-proportioned four-chamber enlargement (Fig 2, *E* and *F*), suggest that this model with modest volume overload triggers a well-compensated adaptive cardiac hypertrophy.

We showed that there was no significant fibrosis, nor change in collagen content 5 weeks after AVF (Fig 3). This finding was confirmed by our RNA sequencing results that showed the upregulation of a number of ECM-related genes including multiple collagen subtypes, collagen processing enzymes, matricellular genes, and various glycoproteins and proteoglycans (Fig 4, *bottom*). The upregulation of multiple ECM genes is not surprising because there was significant LV remodeling and, together with our functional and histologic analyses, suggest that the increase in collagen synthesis was proportional with the degree of cardiac hypertrophy. These results are consistent with prior reports showing upregulation of ECM genes[79] and preserved collagen content after AVF,[80,81] but different from others that showed loss of interstitial LV collagen,[82,83] and yet others that showed increased LV collagen.[84,85] The reasons for the discrepancy in the literature is not clear, but might relate to the degree of volume overload triggered in these various animal models, where those models with severe volume overload resulting in heart failure were more likely to manifest changes in collagen content than those without.

In addition to changes in ECM-related genes, the mRNA sequencing data showed significant changes in expression of cardiac fetal genes, as well as genes implicated in metabolism and ion channels. Increases in cardiac fetal genes are expected given their role in regulating cellular hypertrophy and is believed to be an adaptive process in response to cardiac stress.[86,87] With heart failure, the activation of the fetal gene program is accompanied by a profound alteration in energy metabolism with a decrease in fatty acid oxidation and increased use of carbohydrates.[86] Prior microarray analyses of pressure-overloaded (transverse aortic constriction) and volume-overloaded (aortocaval fistula) rat hearts demonstrated decreases in lipid metabolism and oxidative phosphorylation.[79] Although we report a modest 1.6-fold decrease in transcripts coding for (PPAR)-alpha, a major regulator of genes involved in fatty acid beta-oxidation, other metabolism-related genes previously shown to be downregulated in Barnes et al[79] such as ACSL1, Pecr, Acox1, Acsbg1, Sdhb, and Cox7c were not significantly changed in our data. This result suggests that our model with its more modest volume overload is associated with a less dramatic alteration in cardiac energy metabolism.

Ion channel remodeling has been previously shown to occur in other models of ventricular hypertrophy, with altered potassium, sodium, and calcium currents resulting in prolongation of the action potential duration.[88] Interestingly, we also noted the downregulation of several ion channel transcripts, such as the voltage-gated calcium (Cacna1c), sodium (Scn4a), and potassium (Kcnv2, Kcnh2) channels with AVF-induced LV hypertrophy (Fig 4). Although the electrophysiologic effects of these transcriptional changes remain to be determined, the downregulation of potassium channels in particular has been linked to action potential duration prolongation in hypertrophied rat LV after aortocaval fistulae.[89] Such changes to membrane excitability and action potential morphology might be mechanisms that contribute to the increased arrhythmia and sudden cardiac death seen with severe volume overload in rats,[90] and predicted by the bioinformatics data here (Fig 7). Although patients on hemodialysis have an increased risk of arrhythmia and sudden cardiac death compared with the general population,[91] further studies are needed to clarify the role of AVF-induced cardiac remodeling to the pathogenesis of arrhythmogenicity in these medically complex patients.

Our bioinformatics data suggest that AVF-induced LV hypertrophy is associated with increased inflammation, cellular proliferation, and angiogenesis with potential cardioprotective effects (Figs 5-7). The upregulation of

these processes is expected and likely necessary for adaptive ventricular remodeling, because a hypertrophied myocardium without adequate angiogenesis would lead to a mismatch of supply and demand, ischemia, and fibrosis. The proangiogenic effect of AVF on the heart is suggested by increased activation of multiple angiogenic factors such as Akt1, Erbb2, HGF, and VEGF; increased regional myocardial blood flow was observed in dogs with AVF compared with those without, and was postulated as a mechanism by which AVF decreased the size of induced myocardial infarctions.[92] Another potential mechanism of cardioprotection is the upregulation of proproliferative and prosurvival molecules (Fig 6) that might increase cellular tolerance to ischemia or injury. These results suggest that AVF-induced cardiac remodeling might not be as deleterious as previously thought and might even confer some benefit. Whether AVF-induced cardiac conditioning can be a therapeutic strategy for select cardiac diseases requires further laboratory and clinical investigation.

Limitations. This study has several limitations. We used healthy, young adult mice, and their cardiac response to AVF might be different from older mice with hypertension or renal insufficiency. In addition, although we used the same needle size for AVF creation, we did not quantify the resultant AVF flow rate and thus could not study whether AVF-induced cardiac remodeling showed shunt flow dependence. Furthermore, our model uses a central AVF that could potentially exert different effects on the heart when compared with peripheral AVF used in patients with ESRD, potential flow rate differences notwithstanding. Another limitation is that the bioinformatics analysis was based on RNA sequencing at 10 days postoperatively and therefore does not reflect cellular processes that occur earlier or later. In addition, the transcriptomics was performed from bulk mRNA, reflecting signal transduction of both cardiomyocytes and surrounding cells. Finally, the bioinformatics analysis is only predictive and will require additional investigation to confirm these results.

CONCLUSIONS

AVF in mice stimulates cardiac hypertrophy that is not accompanied by functional decline on imaging or pathologic analyses at 5 weeks postoperatively, suggesting that AVF-induced cardiac remodeling is adaptive and physiologic. The transcriptomics of AVF-induced LV hypertrophy suggests that the molecular signatures of this process are the upregulation of proangiogenic, proproliferative, and prosurvival factors, as well as an electrical remodeling with downregulation of several ion channels. Thus, cardiac remodeling after AVF potentially confers cardioprotective, but also arrhythmogenic effects, highlighting the need for further investigation.

AUTHOR CONTRIBUTIONS

Conception and design: SL, ST, AS, AD
Analysis and interpretation: SL, ST, LG, RT, JL, AS, AD
Data collection: SL, ST, NG, AD
Writing the article: SL, AD
Critical revision of the article: SL, ST, NG, LG, RT, JL, AS, AD
Final approval of the article: SL, ST, NG, LG, RT, JL, AS, AD
Statistical analysis: Not applicable
Obtained funding: Not applicable
Overall responsibility: AD
AS and AD contributed equally to this article and share co-senior authorship

REFERENCES

1. Robbin ML, Chamberlain NE, Lockhart ME, Gallichio MH, Young CJ, Deierhoi MH, et al. Hemodialysis arteriovenous fistula maturity: US evaluation. Radiology 2002;225:59-64.
2. Vascular Access Work G. Clinical practice guidelines for vascular access. Am J Kidney Dis 2006;48(Suppl 1):S176-247.
3. Robbin ML, Greene T, Allon M, Dember LM, Imrey PB, Cheung AK, et al. Prediction of arteriovenous fistula clinical maturation from postoperative ultrasound measurements: findings from the hemodialysis fistula maturation study. J Am Soc Nephrol 2018;29:2735-44.
4. Iwashima Y, Horio T, Takami Y, Inenaga T, Nishikimi T, Takishita S, et al. Effects of the creation of arteriovenous fistula for hemodialysis on cardiac function and natriuretic peptide levels in CRF. Am J Kidney Dis 2002;40:974-82.
5. Ori Y, Korzets A, Katz M, Erman A, Weinstein T, Malachi T, et al. The contribution of an arteriovenous access for hemodialysis to left ventricular hypertrophy. Ame J Kidney Dis 2002;40:745-52.
6. Ye WL, Fang LG, Ma J, Li XM. [Long-term effects of arteriovenous fistula on cardiac structure and function in non-diabetic hemodialysis patients]. Zhongguo yi xue ke xue yuan xue bao. Acta Academiae Medicinae Sinicae 2013;35:95-101.
7. Dundon BK, Torpey K, Nelson AJ, Wong DT, Duncan RF, Meredith IT, et al. The deleterious effects of arteriovenous fistula-creation on the cardiovascular system: a longitudinal magnetic resonance imaging study. Int J Nephrol Renovasc Dis 2014;7:337-45.
8. Reddy YNV, Obokata M, Dean PG, Melenovsky V, Nath KA, Borlaug BA. Long-term cardiovascular changes following creation of arteriovenous fistula in patients with end stage renal disease. Eur Heart J 2017;38:1913-23.
9. Saleh MA, El Kilany WM, Keddis VW, El Said TW. Effect of high flow arteriovenous fistula on cardiac function in hemodialysis patients. Egypt Heart J 2018;70:337-41.
10. Kannel WB. Left ventricular hypertrophy as a risk factor: the Framingham experience. J Hypertens Suppl 1991;9:S3-8; discussion: S8-9.
11. Wei X, Liu X, Rosenzweig A. What do we know about the cardiac benefits of exercise? Trends Cardiovasc Med 2015;25:529-36.
12. Maillet M, van Berlo JH, Molkentin JD. Molecular basis of physiological heart growth: fundamental concepts and new players. Nat Rev Mol Cell Biol 2013;14:38-48.
13. Rao NN, Stokes MB, Rajwani A, Ullah S, Williams K, King D, et al. Effects of arteriovenous fistula ligation on cardiac structure and function in kidney transplant recipients. Circulation 2019;139:2809-18.
14. Scholz SS, Vukadinovic D, Lauder L, Ewen S, Ukena C, Townsend RR, et al. Effects of arteriovenous fistula on blood pressure in patients with end-stage renal disease: a systematic meta-analysis. J Am Heart Assoc 2019;8:e011183.
15. Lobo MD, Ott C, Sobotka PA, Saxena M, Stanton A, Cockcroft JR, et al. Central iliac arteriovenous anastomosis for uncontrolled hypertension: one-year results from the ROX CONTROL HTN trial. Hypertension 2017;70:1099-105.
16. Ott C, Lobo MD, Sobotka PA, Mahfoud F, Stanton A, Cockcroft J, et al. Effect of arteriovenous anastomosis on blood pressure reduction in patients with isolated systolic hypertension compared with combined hypertension. J Am Heart Assoc 2016;5:e004234.
17. Lobo MD, Sobotka PA, Stanton A, Cockcroft JR, Sulke N, Dolan E, et al. Central arteriovenous anastomosis for the treatment of patients

with uncontrolled hypertension (the ROX CONTROL HTN study): a randomised controlled trial. Lancet 2015;385:1634-41.
18. Dhingra RK, Young EW, Hulbert-Shearon TE, Leavey SF, Port FK. Type of vascular access and mortality in U.S. hemodialysis patients. Kidney Int 2001;60:1443-51.
19. Wasse H, Speckman RA, McClellan WM. Arteriovenous fistula use is associated with lower cardiovascular mortality compared with catheter use among ESRD patients. Semin Dial 2008;21:483-9.
20. Ocak G, Halbesma N, le Cessie S, Hoogeveen EK, van Dijk S, Kooman J, et al. Haemodialysis catheters increase mortality as compared to arteriovenous accesses especially in elderly patients. Nephrol Dial Transplant 2011;26:2611-7.
21. Yamamoto K, Protack CD, Tsuneki M, Hall MR, Wong DJ, Lu DY, et al. The mouse aortocaval fistula recapitulates human arteriovenous fistula maturation. Am J Physiol Heart Circ Physiol 2013;305:H1718-25.
22. Hall MR, Yamamoto K, Protack CD, Tsuneki M, Kuwahara G, Assi R, et al. Temporal regulation of venous extracellular matrix components during arteriovenous fistula maturation. J Vasc Access 2015;16:93-106.
23. Scheuermann-Freestone M, Freestone NS, Langenickel T, Hohnel K, Dietz R, Willenbrock R. A new model of congestive heart failure in the mouse due to chronic volume overload. Eur J Heart Fail 2001;3:535-43.
24. Toischer K, Rokita AG, Unsold B, Zhu W, Kararigas G, Sossalla S, et al. Differential cardiac remodeling in preload versus afterload. Circulation 2010;122:993-1003.
25. Yamamoto K, Protack CD, Kuwahara G, Tsuneki M, Hashimoto T, Hall MR, et al. Disturbed shear stress reduces Klf2 expression in arterial-venous fistulae in vivo. Physiol Rep 2015;3:e12348.
26. Yamamoto K, Li X, Shu C, Miyata T, Dardik A. Technical aspects of the mouse aortocaval fistula. J Vis Exp 2013:e50449.
27. Wilkins BJ, Dai YS, Bueno OF, Parsons SA, Xu J, Plank DM, et al. Calcineurin/NFAT coupling participates in pathological, but not physiological, cardiac hypertrophy. Circ Res 2004;94:110-8.
28. DeBosch B, Treskov I, Lupu TS, Weinheimer C, Kovacs A, Courtois M, et al. Akt1 is required for physiological cardiac growth. Circulation 2006;113:2097-104.
29. Kemi OJ, Ceci M, Wisloff U, Grimaldi S, Gallo P, Smith GL, et al. Activation or inactivation of cardiac Akt/mTOR signaling diverges physiological from pathological hypertrophy. J Cell Physiol 2008;214:316-21.
30. Marsh JD, Lehmann MH, Ritchie RH, Gwathmey JK, Green GE, Schiebinger RJ. Androgen receptors mediate hypertrophy in cardiac myocytes. Circulation 1998;98:256-61.
31. Tshori S, Gilon D, Beeri R, Nechushtan H, Kaluzhny D, Pikarsky E, et al. Transcription factor MITF regulates cardiac growth and hypertrophy. J Clin Invest 2006;116:2673-81.
32. Mehta G, Kumarasamy S, Wu J, Walsh A, Liu L, Williams K, et al. MITF interacts with the SWI/SNF subunit, BRG1, to promote GATA4 expression in cardiac hypertrophy. J Mol Cell Cardiol 2015;88:101-10.
33. Sarkar S, Leaman DW, Gupta S, Sil P, Young D, Morehead A, et al. Cardiac overexpression of myotrophin triggers myocardial hypertrophy and heart failure in transgenic mice. J Biol Chem 2004;279:20422-34.
34. Bujak M, Frangogiannis NG. The role of TGF-beta signaling in myocardial infarction and cardiac remodeling. Cardiovasc Res 2007;74:184-95.
35. Dobaczewski M, Chen W, Frangogiannis NG. Transforming growth factor (TGF)-beta signaling in cardiac remodeling. J Mol Cell Cardiol 2011;51:600-6.
36. Bajpai G, Schneider C, Wong N, Bredemeyer A, Hulsmans M, Nahrendorf M, et al. The human heart contains distinct macrophage subsets with divergent origins and functions. Nat Med 2018;24:1234-45.
37. Anzai A, Choi JL, He S, Fenn AM, Nairz M, Rattik S, et al. The infarcted myocardium solicits GM-CSF for the detrimental oversupply of inflammatory leukocytes. J Exp Med 2017;214:3293-310.
38. Zhang J. Yin and yang interplay of IFN-gamma in inflammation and autoimmune disease. J Clin Invest 2007;117:871-3.
39. Beer LA, Kossenkov AV, Liu Q, Luning Prak E, Domchek S, Speicher DW, et al. Baseline immunoglobulin e levels as a marker of doxorubicin- and trastuzumab-associated cardiac dysfunction. Circ Res 2016;119:1135-44.
40. Guo X, Yuan S, Liu Y, Zeng Y, Xie H, Liu Z, et al. Serum IgE levels are associated with coronary artery disease severity. Atherosclerosis 2016;251:355-60.
41. Shintani Y, Ito T, Fields L, Shiraishi M, Ichihara Y, Sato N, et al. IL-4 as a repurposed biological drug for myocardial infarction through augmentation of reparative cardiac macrophages: proof-of-concept data in mice. Sci Rep 2017;7:6877.
42. Zogbi C, Oliveira NC, Levy D, Bydlowski SP, Bassaneze V, Neri EA, et al. Beneficial effects of IL-4 and IL-6 on rat neonatal target cardiac cells. Sci Rep 2020;10:12350.
43. Peng H, Sarwar Z, Yang XP, Peterson EL, Xu J, Janic B, et al. Profibrotic role for interleukin-4 in cardiac remodeling and dysfunction. Hypertension 2015;66:582-9.
44. Sack MN, Smith RM, Opie LH. Tumor necrosis factor in myocardial hypertrophy and ischaemia–an anti-apoptotic perspective. Cardiovasc Res 2000;45:688-95.
45. Matsui T, Rosenzweig A. Convergent signal transduction pathways controlling cardiomyocyte survival and function: the role of PI 3-kinase and Akt. J Mol Cell Cardiol 2005;38:63-71.
46. Shiojima I, Walsh K. Regulation of cardiac growth and coronary angiogenesis by the Akt/PKB signaling pathway. Genes Dev 2006;20:3347-65.
47. Gan J, Tang FMK, Su X, Lu G, Xu J, Lee HSS, et al. microRNA-1 inhibits cardiomyocyte proliferation in mouse neonatal hearts by repressing CCND1 expression. Ann Transl Med 2019;7:455.
48. D'Uva G, Aharonov A, Lauriola M, Kain D, Yahalom-Ronen Y, Carvalho S, et al. ERBB2 triggers mammalian heart regeneration by promoting cardiomyocyte dedifferentiation and proliferation. Nat Cell Biol 2015;17:627-38.
49. Bolte C, Zhang Y, Wang IC, Kalin TV, Molkentin JD, Kalinichenko VV. Expression of Foxm1 transcription factor in cardiomyocytes is required for myocardial development. PloS One 2011;6:e22217.
50. Bolte C, Zhang Y, York A, Kalin TV, Schultz Jel J, Molkentin JD, et al. Postnatal ablation of Foxm1 from cardiomyocytes causes late onset cardiac hypertrophy and fibrosis without exacerbating pressure overload-induced cardiac remodeling. PloS One 2012;7:e48713.
51. Sengupta A, Kalinichenko VV, Yutzey KE. FoxO1 and FoxM1 transcription factors have antagonistic functions in neonatal cardiomyocyte cell-cycle withdrawal and igf1 gene regulation. Circ Res 2013;112:267-77.
52. Rappolee DA, Iyer A, Patel Y. Hepatocyte growth factor and its receptor are expressed in cardiac myocytes during early cardiogenesis. Circ Res 1996;78:1028-36.
53. Roggia C, Ukena C, Bohm M, Kilter H. Hepatocyte growth factor (HGF) enhances cardiac commitment of differentiating embryonic stem cells by activating PI3 kinase. Exp Cell Res 2007;313:921-30.
54. Li J, Gao E, Vite A, Yi R, Gomez L, Goossens S, et al. Alpha-catenins control cardiomyocyte proliferation by regulating yap activity. Circ Res 2015;116:70-9.
55. Flink IL, Oana S, Maitra N, Bahl JJ, Morkin E. Changes in E2F complexes containing retinoblastoma protein family members and increased cyclin-dependent kinase inhibitor activities during terminal differentiation of cardiomyocytes. J Mol Cell Cardiol 1998;30:563-78.
56. Yuan X, Braun T. Multimodal regulation of cardiac myocyte proliferation. Circ Res 2017;121:293-309.
57. Schips TG, Wietelmann A, Hohn K, Schimanski S, Walther P, Braun T, et al. FoxO3 induces reversible cardiac atrophy and autophagy in a transgenic mouse model. Cardiovasc Res 2011;91:587-97.
58. Cao DJ, Jiang N, Blagg A, Johnstone JL, Gondalia R, Oh M, et al. Mechanical unloading activates FoxO3 to trigger Bnip3-dependent cardiomyocyte atrophy. J Am Heart Assoc 2013;2:e000016.
59. Bao MH, Feng X, Zhang YW, Lou XY, Cheng Y, Zhou HH. Let-7 in cardiovascular diseases, heart development and cardiovascular differentiation from stem cells. Int J Mol Sci 2013;14:23086-102.
60. Kuppusamy KT, Jones DC, Sperber H, Madan A, Fischer KA, Rodriguez ML, et al. Let-7 family of microRNA is required for maturation and adult-like metabolism in stem cell-derived cardiomyocytes. Proc Natl Acad Sci U S A 2015;112:E2785-94.
61. Wang X, Wang HX, Li YL, Zhang CC, Zhou CY, Wang L, et al. MicroRNA Let-7i negatively regulates cardiac inflammation and fibrosis. Hypertension 2015;66:776-85.

62. Zhou X, Sun F, Luo S, Zhao W, Yang T, Zhang G, et al. Let-7a is an antihypertrophic regulator in the heart via targeting calmodulin. Int J Biol Sci 2017;13:22-31.
63. Wang S, Zhou H, Wu D, Ni H, Chen Z, Chen C, et al. MicroRNA let-7a regulates angiogenesis by targeting TGFBR3 mRNA. J Cell Mol Med 2019;23:556-67.
64. Banjo T, Grajcarek J, Yoshino D, Osada H, Miyasaka KY, Kida YS, et al. Haemodynamically dependent valvulogenesis of zebrafish heart is mediated by flow-dependent expression of miR-21. Nat Commun 2013;4:1978.
65. Gupta SK, Itagaki R, Zheng X, Batkai S, Thum S, Ahmad F, et al. miR-21 promotes fibrosis in an acute cardiac allograft transplantation model. Cardiovasc Res 2016;110:215-26.
66. Yuan J, Chen H, Ge D, Xu Y, Xu H, Yang Y, et al. iR-21 promotes cardiac fibrosis after myocardial infarction via targeting smad7. Cell Physiol Biochem 2017;42:2207-19.
67. Oka T, Akazawa H, Naito AT, Komuro I. Angiogenesis and cardiac hypertrophy: maintenance of cardiac function and causative roles in heart failure. Circ Res 2014;114:565-71.
68. Ackah E, Yu J, Zoellner S, Iwakiri Y, Skurk C, Shibata R, et al. Akt1/protein kinase Balpha is critical for ischemic and VEGF-mediated angiogenesis. J Clin Invest 2005;115:2119-27.
69. Kumar R, Yarmand-Bagheri R. The role of HER2 in angiogenesis. Semin Oncol 2001;28:27-32.
70. Bussolino F, Di Renzo MF, Ziche M, Bocchietto E, Olivero M, Naldini L, et al. Hepatocyte growth factor is a potent angiogenic factor which stimulates endothelial cell motility and growth. J Cell Biol 1992;119:629-41.
71. Ahmet I, Sawa Y, Iwata K, Matsuda H. Gene transfection of hepatocyte growth factor attenuates cardiac remodeling in the canine heart: a novel gene therapy for cardiomyopathy. J Thorac Cardiovasc Surg 2002;124:957-63.
72. Matsui T, Tao J, del Monte F, Lee KH, Li L, Picard M, et al. Akt activation preserves cardiac function and prevents injury after transient cardiac ischemia in vivo. Circulation 2001;104:330-5.
73. Koeppen M, Lee JW, Seo SW, Brodsky KS, Kreth S, Yang IV, et al. Hypoxia-inducible factor 2-alpha-dependent induction of amphiregulin dampens myocardial ischemia-reperfusion injury. Nat Commun 2018;9:816.
74. Ueda H, Nakamura T, Matsumoto K, Sawa Y, Matsuda H, Nakamura T. A potential cardioprotective role of hepatocyte growth factor in myocardial infarction in rats. Cardiovasc Res 2001;51:41-50.
75. Okayama K, Azuma J, Dosaka N, Iekushi K, Sanada F, Kusunoki H, et al. Hepatocyte growth factor reduces cardiac fibrosis by inhibiting endothelial-mesenchymal transition. Hypertension 2012;59:958-65.
76. Shiojima I, Sato K, Izumiya Y, Schiekofer S, Ito M, Liao R, et al. Disruption of coordinated cardiac hypertrophy and angiogenesis contributes to the transition to heart failure. J Clin Invest 2005;115:2108-18.
77. Liu L, Jin X, Hu CF, Zhang YP, Zhou Z, Li R, et al. Amphiregulin enhances cardiac fibrosis and aggravates cardiac dysfunction in mice with experimental myocardial infarction partly through activating EGFR-dependent pathway. Basic Res Cardiol 2018;113:12.
78. Ryan TD, Rothstein EC, Aban I, Tallaj JA, Husain A, Lucchesi PA, et al. Left ventricular eccentric remodeling and matrix loss are mediated by bradykinin and precede cardiomyocyte elongation in rats with volume overload. J Am Coll Cardiol 2007;49:811-21.
79. Barnes J, Pat B, Chen YW, Powell PC, Bradley WE, Zheng J, et al. Whole-genome profiling highlights the molecular complexity underlying eccentric cardiac hypertrophy. Ther Adv Cardiovasc Dis 2014;8:97-118.
80. Weber KT, Pick R, Silver MA, Moe GW, Janicki JS, Zucker IH, et al. Fibrillar collagen and remodeling of dilated canine left ventricle. Circulation 1990;82:1387-401.
81. Namba T, Tsutsui H, Tagawa H, Takahashi M, Saito K, Kozai T, et al. Regulation of fibrillar collagen gene expression and protein accumulation in volume-overloaded cardiac hypertrophy. Circulation 1997;95:2448-54.
82. El Hajj MC, Ninh VK, El Hajj EC, Bradley JM, Gardner JD. Estrogen receptor antagonism exacerbates cardiac structural and functional remodeling in female rats. Am J Physiol Heart Circ Physiol 2017;312:H98-105.
83. Ruzicka M, Keeley FW, Leenen FH. The renin-angiotensin system and volume overload-induced changes in cardiac collagen and elastin. Circulation 1994;90:1989-96.
84. El Hajj EC, El Hajj MC, Ninh VK, Gardner JD. Inhibitor of lysyl oxidase improves cardiac function and the collagen/MMP profile in response to volume overload. Am J Physiol Heart Circ Physiol 2018;315:H463-73.
85. Brower GL, Janicki JS. Contribution of ventricular remodeling to pathogenesis of heart failure in rats. Am J Physiol Heart Circ Physiol 2001;280:H674-83.
86. Taegtmeyer H, Sen S, Vela D. Return to the fetal gene program: a suggested metabolic link to gene expression in the heart. Ann N Y Acad Sci 2010;1188:191-8.
87. Rajabi M, Kassiotis C, Razeghi P, Taegtmeyer H. Return to the fetal gene program protects the stressed heart: a strong hypothesis. Heart Fail Rev 2007;12:331-43.
88. Tomaselli GF, Marban E. Electrophysiological remodeling in hypertrophy and heart failure. Cardiovasc Res 1999;42:270-83.
89. Sedmera D, Neckar J, Benes J Jr, Pospisilova J, Petrak J, Sedlacek K, et al. Changes in myocardial composition and conduction properties in rat heart failure model induced by chronic volume overload. Front Physiol 2016;7:367.
90. Melenovsky V, Skaroupkova P, Benes J, Torresova V, Kopkan L, Cervenka L. The course of heart failure development and mortality in rats with volume overload due to aorto-caval fistula. Kidney Blood Press Res 2012;35:167-73.
91. Makar MS, Pun PH. Sudden cardiac death among hemodialysis patients. Am J Kidney Dis 2017;69:684-95.
92. Mahgoub MA, Guo JH, Gao SP, Taher MM, Salter DD, Wechsler AS, et al. Hyperdynamic circulation of arteriovenous fistula preconditions the heart and limits infarct size. Ann Thorac Surg 1999;68:22-8.

Submitted Feb 16, 2021; accepted May 11, 2021.

APPENDIX.

Primer list

Gene	Forward Primer	Reverse Primer
PPARa	AGAGCCCCATCTGTCCTCTC	ACTGGTAGTCTGCAAAACCAAA
PPARGC1	TATGGAGTGACATAGAGTGTGCT	CCACTTCAATCCACCCAGAAAG
PPP3Ca	GTGAAAGCCGTTCCATTTCCA	GAATCGAAGCACCCTCTGTTATT
Akt1	ATGAACGACGTAGCCATTGTG	TTGTAGCCAATAAAGGTGCCAT
VEGFa	GCACATAGAGAGAATGAGCTTCC	CTCCGCTCTGAACAAGGCT
IRS1	CGATGGCTTCTCAGACGTG	CAGCCCGCTTGTTGATGTTG
HIF1a	ACCTTCATCGGAAACTCCAAAG	ACTGTTAGGCTCAGGTGAACT
GPX1	AGTCCACCGTGTATGCCTTCT	GAGACGCGACATTCTCAATGA
MMP2	CAAGTTCCCCGGCGATGTC	TTCTGGTCAAGGTCACCTGTC
IGF1R	CATGTGCTGGCAGTATAACCC	TCGGGAGGCTTGTTCTCCT
MYH7	ACTGTCAACACTAAGAGGGTCA	TTGGATGATTTGATCTTCCAGGG
FN1	TTCAAGTGTGATCCCCATGAAG	CAGGTCTACGGCAGTTGTCA
NPPA	GCTTCCAGGCCATATTGGAG	GGGGGCATGACCTCATCTT
TIMP1	GCAACTCGGACCTGGTCATAA	CGGCCCGTGATGAGAAACT
B2M	CATGGCTCGCTCGGTGAC	CAGTTCAGTATGTTCGGCTTCC

Quantitative real-time polymerase chain reaction

Freshly excised left ventricles were snap frozen in liquid nitrogen, and RNA was then extracted and purified using the RNeasy Mini Kit (Qiagen). cDNA was synthesized using the SuperScript III system (Thermo Fisher Scientific), and quantitative PCR was performed with SYBR Green (Bio-Rad) in the CFX96 Touch Real-Time PCR Detection System (Bio-Rad). Primers used for the various genes of interest are included in the table above. Gene expression levels were normalized to β2-microglobulin.

Quantification of collagen content with picrosirius red

Hearts from sham (male, n = 3, female, n = 3) and AVF (male, n = 4, female, n = 3) mice were excised at post-operative week 5, rinsed with normal saline solution, and immersed in 10% neutralized buffered formalin for 24-48 hours. The tissue block was then embedded in paraffin and cut in 5 μm cross-sections. Picrosirius red staining was used to assess collagen content and identify areas of fibrosis at both low and high magnification. Quantification of relative collagen content was performed in high-powered (400x) coronal sections for each of the 4 cardiac chambers, using an automated custom Matlab (MathWorks, Natick MA) algorithm that quantifies the intensity of red saturation per μm^2.

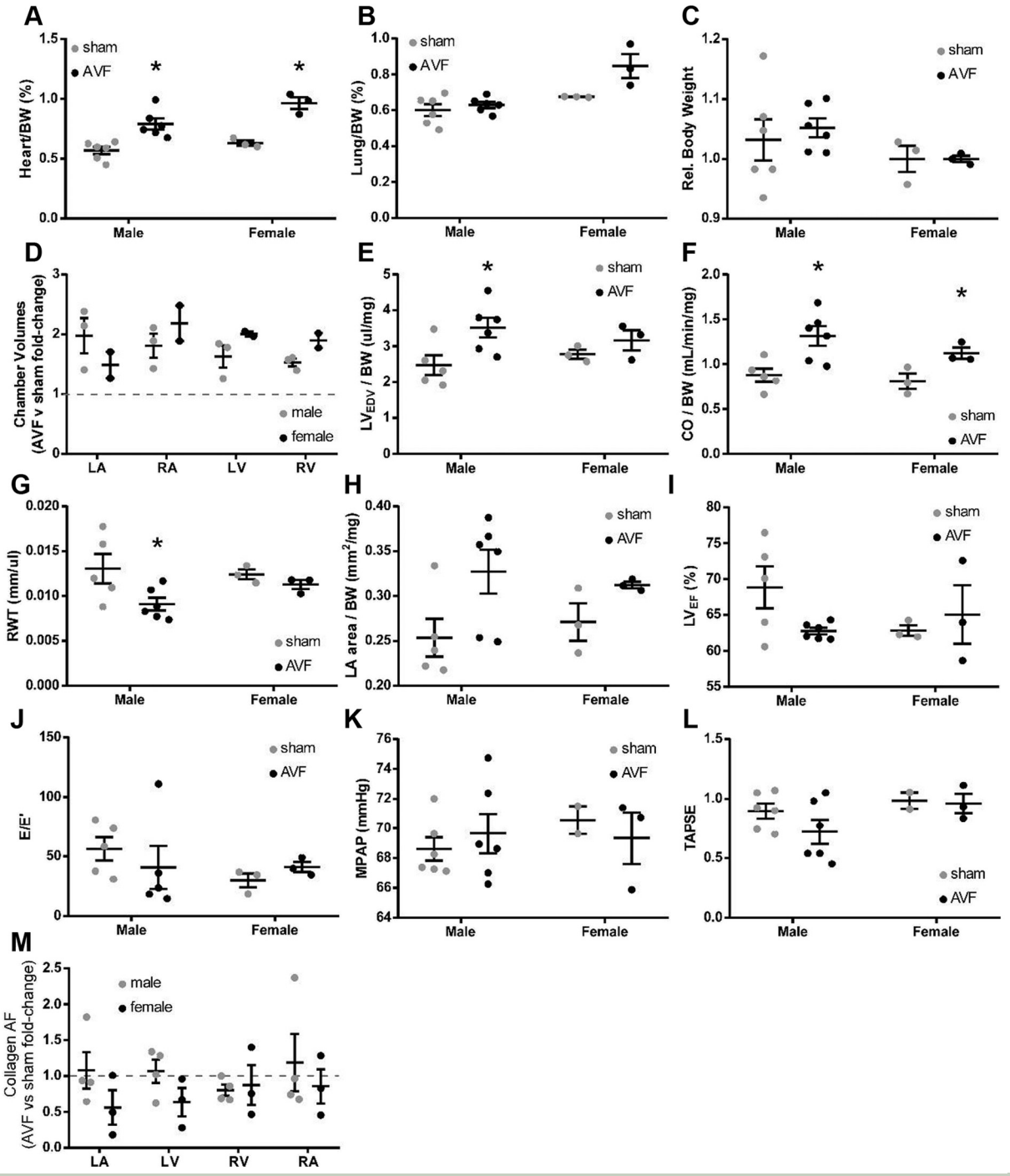

Supplementary Fig 1. Structural and functional cardiac changes 5 weeks after arteriovenous fistulae (*AVF*) or sham surgery stratified by sex. **A,** Whole heart mass normalized to body weight was increased after AVF (male [n = 6 each], $P = .002$; female [n = 3 each], $P = .003$). **B,** Normalized lung weights (male, $P = .45$; female, $P = .06$), and relative body weights **(C)** (male, $P = .6$; female, 1.0). were also unchanged for AVF versus sham. **D,** Relative chamber volumes (AVF:sham) as measured by computed tomography angiography (CTA) were not significantly different (left atrium [*LA*], $P = .32$; right atrium [*RA*], $P = .35$; left ventricle [*LV*], $P = .21$; right ventricle [*RV*], $P = .06$) between male (n = 3 each) and female (n = 2 each). **E-L**, Echo indices show similar trends for males (n = 5-6 each) and females (n = 3 each), LV end diastolic volume [LV_{EDV}]/body weight [*BW*] (male, $P = .03$; female, $P = .28$); cardiac output normalized to BW [*CO/BW*] (male, $P = .01$; female, $P = .04$); relative wall thickness (*RWT*) (male, $P = .04$; female, $P = .21$); LA_{area}/BW (male, $P = .05$; female, $P = .12$); LV_{EF} (male, $P = .92$; female, $P = .62$); E/E′, (male, $P = .47$; female, $P = .19$); mean pulmonary artery pressure (*MPAP*) (male, $P = .51$; female, $P = .64$); tricuspid annular plane systolic excursion (*TAPSE*) (male, $P = .17$; female, $P = .85$). **M**, Relative change in collagen area fraction (AVF:sham) was not significantly different between male (n = 4 each) and female (n = 3 each), LA, $P = .21$; RA, $P = .55$; LV, $P = .15$; RV, $P = .79$.

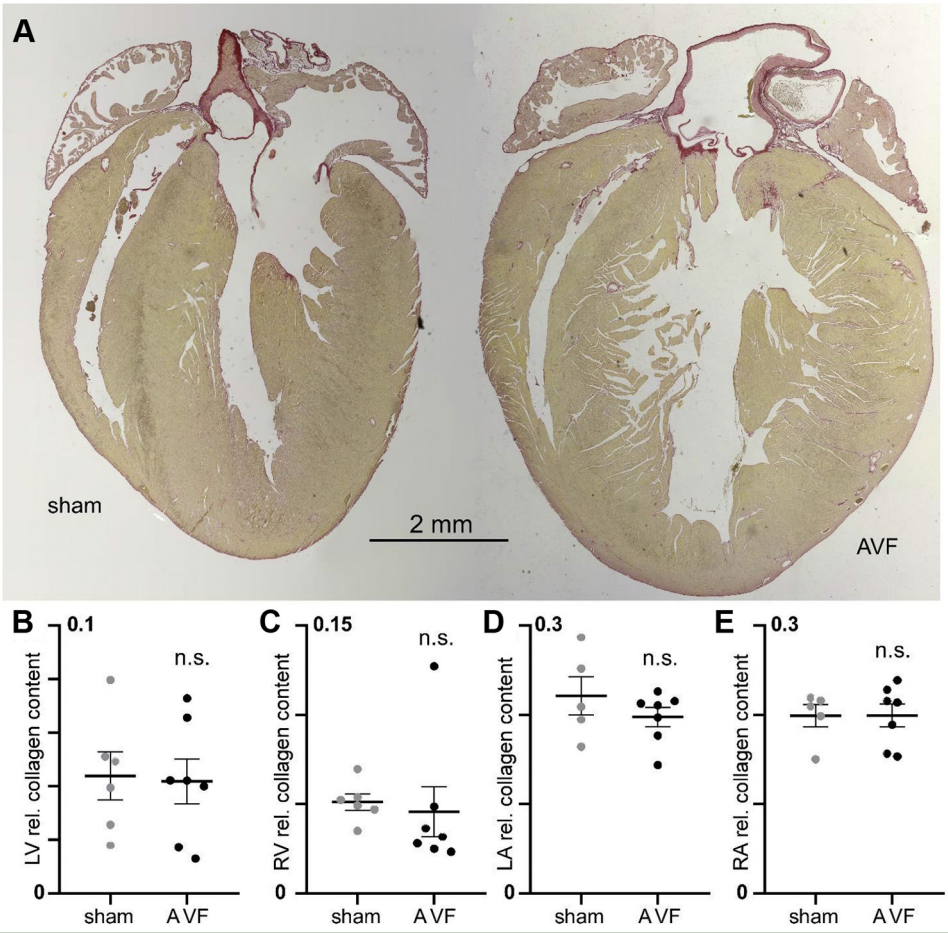

Supplementary Fig 2. Preserved cardiac collagen content 5 weeks after arteriovenous fistulae (*AVF*) or sham surgery. **A,** Exemplar sham (*left*) and AVF (*right*) coronal cardiac sections stained with picrosirius red (colors collagen red). **B-E,** Summary data (sham, n = 5-6; AVF, n = 7) of quantitation of relative collagen content (degree of redness/unit area) show no significant difference between sham and AVF across all four chambers (left ventricle [*LV*], *P* = .87; right ventricle [*RV*], *P* = .74; left atrium [*LA*]: *P* = .31; right atrium (*RA*), *P* = .98).

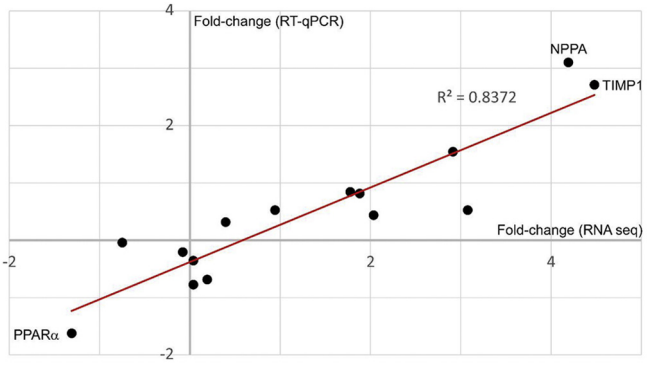

Supplementary Fig 3. Comparison of gene expression quantitation by quantitative real-time polymerase chain reaction (*qRT-PCR*) versus RNA sequencing. Genes interrogated were: PPARa, Ppargc1, PPP3Ca, Akt1, Vegfa, Irs1, Hif1a, Gpx1, Mmp2, Igf1R, Myh7, Fn1, Nppa, and Timp1. Housekeeping gene used for qRT-PCR normalization was β2-microglobulin.

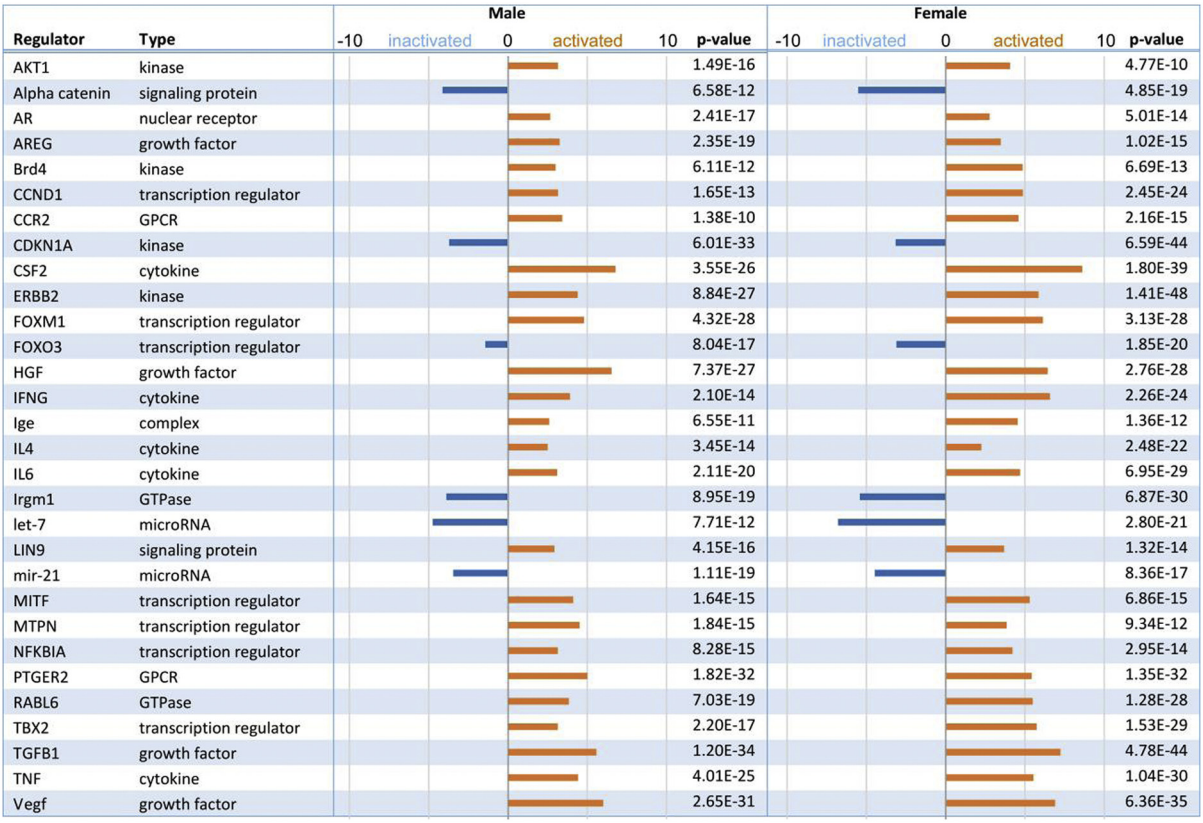

Regulator	Type	Male p-value	Female p-value
AKT1	kinase	1.49E-16	4.77E-10
Alpha catenin	signaling protein	6.58E-12	4.85E-19
AR	nuclear receptor	2.41E-17	5.01E-14
AREG	growth factor	2.35E-19	1.02E-15
Brd4	kinase	6.11E-12	6.69E-13
CCND1	transcription regulator	1.65E-13	2.45E-24
CCR2	GPCR	1.38E-10	2.16E-15
CDKN1A	kinase	6.01E-33	6.59E-44
CSF2	cytokine	3.55E-26	1.80E-39
ERBB2	kinase	8.84E-27	1.41E-48
FOXM1	transcription regulator	4.32E-28	3.13E-28
FOXO3	transcription regulator	8.04E-17	1.85E-20
HGF	growth factor	7.37E-27	2.76E-28
IFNG	cytokine	2.10E-14	2.26E-24
Ige	complex	6.55E-11	1.36E-12
IL4	cytokine	3.45E-14	2.48E-22
IL6	cytokine	2.11E-20	6.95E-29
Irgm1	GTPase	8.95E-19	6.87E-30
let-7	microRNA	7.71E-12	2.80E-21
LIN9	signaling protein	4.15E-16	1.32E-14
mir-21	microRNA	1.11E-19	8.36E-17
MITF	transcription regulator	1.64E-15	6.86E-15
MTPN	transcription regulator	1.84E-15	9.34E-12
NFKBIA	transcription regulator	8.28E-15	2.95E-14
PTGER2	GPCR	1.82E-32	1.35E-32
RABL6	GTPase	7.03E-19	1.28E-28
TBX2	transcription regulator	2.20E-17	1.53E-29
TGFB1	growth factor	1.20E-34	4.78E-44
TNF	cytokine	4.01E-25	1.04E-30
Vegf	growth factor	2.65E-31	6.36E-35

Supplementary Fig 4. Predicted upstream regulators of arteriovenous fistulae (AVF)-induced LV hypertrophy stratified by sex (male, n = 3 each; female, n = 3 each).

Supplementary Table. Select genes from Fig 4 stratified by sex (male, n = 3 each; female, n = 3 each)

	Male				Female				Male vs female		
Gene	Counts	*P* value	FDR	Fold	Counts	*P* value	FDR	Fold	*P* value	FDR	Fold
Cardiac fetal genes											
Nppa	71866	1.07E−06	**2.63E−04**	**4.27**	122990	2.95E−09	**1.29E−07**	**7.73**	1.38E−01	3.19E−01	−1.77
Nppb	98295	5.13E−07	**1.50E−04**	**4.19**	47760	1.22E−10	**8.28E−09**	**2.73**	7.68E−04	**1.40E−02**	**2.42**
Rcan1	33523	6.85E−04	**2.12E−02**	**2.01**					1.42E−01	3.26E−01	1.34
Acta1	356205	2.30E−06	**3.91E−04**	**4.89**	260686	3.10E−10	**1.78E−08**	**6.28**	4.07E−01	6.14E−01	1.39
Atp2a2	3194494	1.01E−03	**2.81E−02**	**−1.52**					4.69E−02	1.64E−01	1.23
Myh6									5.78E−01	7.46E−01	−1.07
Adora1									1.18E−02	7.24E−02	−1.25
Ankrd1	403787	9.47E−06	**1.05E−03**	**2.80**	357243	2.14E−05	**2.43E−04**	**3.29**	5.63E−01	7.36E−01	1.15
Chrm2	24801	6.68E−04	**2.08E−02**	**−1.38**					2.55E−01	4.66E−01	1.15
Meox1	8604	9.80E−13	**3.10E−09**	**2.92**	9552	5.75E−16	**1.58E−13**	**3.94**	5.34E−01	7.15E−01	−1.12
Metabolism											
Ppara	22776	1.29E−07	**5.50E−05**	**−1.58**					4.61E−01	6.60E−01	−1.08
Ion channels											
Kcnh2	21023	1.50E−06	**3.07E−04**	**−1.65**					7.51E−02	2.19E−01	−1.14
Scn4a	11534	1.93E−05	**1.71E−03**	**−1.96**					1.66E−01	3.59E−01	1.22
Kcnv2	2101	3.68E−07	**1.16E−04**	**−3.25**	2422	1.12E−11	**1.03E−09**	**−4.25**	6.14E−01	7.72E−01	1.14
Cacna1c	50394	1.57E−03	**3.78E−02**	**−1.58**					7.62E−01	8.66E−01	−1.03
ECM											
Col1a1	29037	3.72E−03	6.77E−02	2.37	71708	7.89E−18	**3.20E−15**	**3.52**	2.58E−04	**7.07E−03**	**−2.59**
Col1a2	32352	4.60E−03	7.65E−02	2.29	68124	2.88E−16	**8.55E−14**	**3.09**	2.20E−03	**2.66E−02**	**−2.17**
Col3a1	67522	8.54E−05	**5.02E−03**	**2.78**	156350	1.43E−25	**4.41E−22**	**3.34**	1.50E−04	**5.02E−03**	**−2.30**
Col4a1	191475	5.30E−03	8.29E−02	2.33	256819	3.43E−16	**9.97E−14**	**2.60**	2.82E−01	4.95E−01	−1.31
Col4a3	1493	1.21E−04	**6.54E−03**	**3.03**	1779	7.84E−08	**2.06E−06**	**2.57**	7.58E−01	8.64E−01	−1.08
Col5a1	13956	7.31E−03	1.02E−01	2.14	28510	1.64E−24	**3.15E−21**	**3.11**	1.15E−03	**1.81E−02**	**−2.15**
Col5a2	8809	8.75E−05	**5.10E−03**	**3.36**	19440	2.84E−16	**8.55E−14**	**3.53**	5.81E−03	**4.75E−02**	**−2.12**
Col5a3	5542	4.09E−03	7.15E−02	2.50					1.54E−02	8.44E−02	−1.87
Col6a1					35325	1.03E−20	**7.91E−18**	**2.20**	9.03E−03	6.15E−02	−1.72
Col6a2					40195	1.14E−15	**2.84E−13**	**2.11**	2.07E−02	1.00E−01	−1.65
Col8a1	10590	1.23E−05	**1.26E−03**	**3.58**	17855	4.04E−25	**1.04E−21**	**4.99**	3.95E−02	1.48E−01	−1.70
Col12a1	585	1.92E−07	**7.40E−05**	**7.61**	1388	6.16E−03	**2.60E−02**	**4.79**	1.57E−01	3.45E−01	−2.10
Col14a1	3235	2.82E−04	**1.13E−02**	**2.79**	10675	5.32E−20	**3.41E−17**	**2.48**	9.20E−07	**1.09E−04**	**−3.02**
Col15a1	33247	5.23E−03	8.21E−02	2.20	55821	6.01E−14	**1.04E−11**	**2.12**	4.98E−02	1.69E−01	−1.57
Col16a1	1682	1.88E−03	**4.27E−02**	**2.84**	4141	2.10E−07	**4.78E−06**	**2.84**	5.88E−03	**4.77E−02**	**−2.33**
Col18a1	5612	4.62E−03	7.65E−02	2.54	10247	5.07E−12	**5.31E−10**	**3.21**	3.78E−02	1.45E−01	−1.84
Col26a1	161	2.03E−03	**4.50E−02**	**3.87**	489	1.32E−13	**2.04E−11**	**10.85**	8.65E−04	**1.51E−02**	**−3.26**
Lox	1663	4.25E−04	**1.49E−02**	**2.90**	3241	8.50E−07	**1.61E−05**	**7.28**	1.36E−02	7.91E−02	−2.18
Mmp2									4.49E−02	1.60E−01	−1.52
Mmp14	6335	1.15E−03	**3.09E−02**	**2.34**	12447	7.79E−14	**1.29E−11**	**2.64**	3.13E−03	**3.29E−02**	**−1.93**
Mmp23	1506	3.87E−04	**1.40E−02**	**1.97**	1980	1.03E−04	**8.86E−04**	**2.04**	2.57E−01	4.68E−01	−1.25
Timp1	846	6.21E−06	**7.74E−04**	**4.72**	1252	4.31E−04	**2.93E−03**	**4.94**	3.45E−01	5.58E−01	−1.40
Acta1	356205	2.30E−06	**3.91E−04**	**4.89**	260686	3.10E−10	**1.78E−08**	**6.28**	4.07E−01	6.14E−01	1.39
Eln	12218	3.06E−07	**1.05E−04**	**4.10**	21809	1.04E−17	**4.09E−15**	**3.46**	4.31E−02	1.56E−01	−1.63
Vim	71840	1.83E−06	**3.52E−04**	**2.10**	105393	9.40E−13	**1.17E−10**	**2.89**	1.33E−02	7.81E−02	−1.52
Ctgf	19314	3.89E−09	**3.41E−06**	**2.95**	18293	1.19E−07	**2.96E−06**	**2.34**	3.65E−01	5.77E−01	1.19
Fbln2					31515	9.89E−11	**6.99E−09**	**2.18**	5.20E−02	1.74E−01	−1.52
Postn	22726	1.83E−08	**1.20E−05**	**6.41**	64094	4.36E−10	**2.45E−08**	**11.00**	1.37E−02	7.93E−02	−2.83
Sparc	186248	9.05E−13	**3.10E−09**	**2.61**	215083	6.48E−34	**8.54E−30**	**3.83**	1.57E−01	3.45E−01	−1.20
Tnc	741	3.84E−06	**5.82E−04**	**5.48**	2990	3.40E−05	**3.58E−04**	**11.73**	7.15E−03	5.36E−02	−4.17
Bgn	63803	1.57E−03	**3.78E−02**	**2.14**	110150	3.82E−13	**5.21E−11**	**2.44**	9.96E−03	6.58E−02	−1.70
Cd44	3254	9.92E−05	**5.55E−03**	**1.87**					4.17E−01	6.23E−01	−1.12

(Continued on next page)

Supplementary Table. Continued.

	Male				Female				Male vs female		
Gene	Counts	*P* value	FDR	Fold	Counts	*P* value	FDR	Fold	*P* value	FDR	Fold
Fbn1	23402	5.43E−05	**3.57E−03**	**2.81**	44261	2.62E−23	**4.05E−20**	**3.27**	4.09E−03	**3.85E−02**	**−1.86**
Fn1	17289	8.68E−04	**2.50E−02**	**2.90**	35697	3.57E−16	**1.02E−13**	**4.06**	9.91E−03	6.56E−02	−2.11
Lama5	23380	4.59E−04	**1.56E−02**	**−1.67**					1.54E−02	8.44E−02	−1.33
Lum	10039	7.49E−04	**2.25E−02**	**1.87**					9.13E−03	6.19E−02	−1.50
Vcan	3632	7.89E−04	**2.32E−02**	**2.63**	7114	3.93E−07	**8.27E−06**	**2.33**	2.41E−02	1.10E−01	−1.79

FDR, False discovery rate.
Boldface entries indicate statistical significance.